

Toxoplasma gondii TgIST co-opts host chromatin repressors dampening STAT1-dependent gene regulation and IFN- γ -mediated host defenses

Gabrielle Gay,^{1*} Laurence Braun,^{1*} Marie-Pierre Brenier-Pinchart,¹ Julien Vollaire,³ Véronique Josserand,³ Rose-Laurence Bertini,¹ Aurélie Varesano,¹ Bastien Touquet,² Pieter-Jan De Bock,⁴ Yohann Coute,⁴ Isabelle Tardieux,² Alexandre Bougdour,¹ and Mohamed-Ali Hakimi¹

¹Institute for Advanced Biosciences (IAB), Team Host-Pathogen Interactions and Immunity to Infection and ²IAB, Team Membrane and Cell Dynamics of Host-Parasite Interactions, INSERM U1209, CNRS UMR5309, Université Grenoble Alpes, F-38700 Grenoble, France

³IAB, OPTIMAL Small Animal Imaging Facility, 38000 Grenoble, France

⁴Institut de Biosciences et Biotechnologies de Grenoble-Laboratoire Biologie à Grande Échelle (BIG-BGE), Commissariat à l'énergie atomique et aux énergies alternatives (CEA), INSERM, 38000 Grenoble, France

An early hallmark of *Toxoplasma gondii* infection is the rapid control of the parasite population by a potent multifaceted innate immune response that engages resident and homing immune cells along with pro- and counter-inflammatory cytokines. In this context, IFN- γ activates a variety of *T. gondii*-targeting activities in immune and nonimmune cells but can also contribute to host immune pathology. *T. gondii* has evolved mechanisms to timely counteract the host IFN- γ defenses by interfering with the transcription of IFN- γ -stimulated genes. We now have identified TgIST (*T. gondii* inhibitor of STAT1 transcriptional activity) as a critical molecular switch that is secreted by intracellular parasites and traffics to the host cell nucleus where it inhibits STAT1-dependent proinflammatory gene expression. We show that TgIST not only sequesters STAT1 on dedicated loci but also promotes shaping of a nonpermissive chromatin through its capacity to recruit the nucleosome remodeling deacetylase (NuRD) transcriptional repressor. We found that during mice acute infection, *TgIST*-deficient parasites are rapidly eliminated by the homing Gr1⁺ inflammatory monocytes, thus highlighting the protective role of TgIST against IFN- γ -mediated killing. By uncovering TgIST functions, this study brings novel evidence on how *T. gondii* has devised a molecular weapon of choice to take control over a ubiquitous immune gene expression mechanism in metazoans, as a way to promote long-term parasitism.

INTRODUCTION

Toxoplasmosis is a widespread foodborne infection in humans that poses significant public health problems, being recognized as a leading cause of foodborne deaths in the United States (Scallan et al., 2015). Caused by the protozoan *Apicomplexa* parasite *Toxoplasma gondii*, toxoplasmosis, a usually mild disease, in immunocompetent humans can turn into a major threat in immunocompromised patients who experience lethal or chronic cardiac, pulmonary, or cerebral pathologies. Complications of toxoplasmosis are tightened to the capacity of the parasite to differentiate into a quasi-cryptic persistent stage (i.e., bradyzoite) within deep tissue reservoirs and to inflict irreversible damages while differentiating back to the replicative stage (i.e., tachyzoite; Sullivan and Jeffers,

2012). It is during the initial and acute phase of the infection that the tachyzoite-bradyzoite transition occurs in a minor subpopulation while concurring with the massive destruction of the bulk tachyzoite population as a result of a rapid Th1 cell-mediated and short-term proinflammatory response. In this context, IL-12, TNF, and IFN- γ cytokines act at the frontline of defenses against *T. gondii*, with IFN- γ also guaranteeing long-term persistence. Conversely, decline of IFN- γ level correlates with cerebral toxoplasmosis in AIDS patients (Pereira-Chioccola et al., 2009; Meira et al., 2014), whereas genetic loss of IFN- γ renders mice extremely susceptible to toxoplasmosis (Yap and Sher, 1999).

Importantly, counterbalancing of the effect of proinflammatory cytokines is equally essential to the immune response homeostasis and to parasitism, as it prevents immunopathology but preserves host and parasite survival. In line with these requirements, *T. gondii* has found ways to timely

*G. Gay and L. Braun contributed equally to this paper.

Correspondence to Mohamed-Ali Hakimi: mohamed-ali.hakimi@inserm.fr

Abbreviations used: ChIP, chromatin immunoprecipitation; CtBP, C-terminal-binding protein; GAS, gamma activated sequence; HAT, histone acetyltransferase; HDACi, HDAC inhibitor; HFF, human foreskin fibroblast; IFA, immunofluorescence analysis; IRG, immunity-related GTPase; NuRD, nucleosome remodeling deacetylase; p.i., post-infection; PVM, parasitophorous vacuole membrane; TFBS, transcription factor binding site; TgIST, *T. gondii* inhibitor of STAT1 transcriptional activity.

© 2016 Gay et al. This article is distributed under the terms of an Attribution-Noncommercial-Share Alike-No Mirror Sites license for the first six months after the publication date (see <http://www.rupress.org/terms>). After six months it is available under a Creative Commons License (Attribution-Noncommercial-Share Alike 3.0 Unported license, as described at <http://creativecommons.org/licenses/by-nc-sa/3.0/>).

modulate host responsiveness to proinflammatory cytokines. A leading strategy relies on the delivery of parasite effector proteins inside host cells that interplay with host cell signaling pathways—in priority those related to IFN- γ production—by coopting host transcription factors and gaining control overexpression of immune-related genes (Melo et al., 2011; Sturge and Yarovinsky, 2014; Hakimi and Bougdour, 2015).

Considering STAT1 transcription factor as the main signal transducer of the IFN- γ response to *T. gondii* infection (Zimmermann et al., 2006; Kim et al., 2007; Lang et al., 2012; Schneider et al., 2013; Rosowski et al., 2014), we could expect *T. gondii* to design antagonists of the STAT1-positive activity on gene expression as a way to modulate IFN- γ downstream effects. In support of this scheme, in vitro preinfection of nonhematopoietic and hematopoietic cells with tachyzoites, regardless of their genotypes, impedes the IFN- γ -stimulated STAT1-mediated gene expression program, hence preventing expression of MHC class II molecules, IRF1, iNOS/Nos2, class II transactivator (CIITA), interferon-inducible GTPases, and chemokines (CXCL9 and CXCL10; Scharton-Kersten et al., 1997; Lüder et al., 2003; Kim et al., 2007; Lang et al., 2012; Rosowski and Saeij, 2012). However, despite an intensive search, how *T. gondii* interferes with STAT1 function still remains enigmatic.

STAT1 cycles between the cell membrane/cytoplasm and the nucleus. Initiated by IFN- γ binding to the IFN- γ receptor (IFN- γ R), the pool of IFN- γ R-associated STAT1 becomes phosphorylated on Y701 residue (STAT1 Y701-P) by the JAK kinases and is subsequently released in the cytoplasm where it homodimerizes (Ramana et al., 2000; Stark and Darnell, 2012). STAT1 Y701-P dimers translocate to the nucleus and regulate gene expression by binding specifically to gamma activated sequence (GAS) elements in the promoters of primary IFN- γ -responsive genes, in particular the interferon regulatory factor 1 gene (IRF1). IRF1 acts in concert with STAT1 Y701-P to activate secondary response genes (Honda and Taniguchi, 2006). The transcriptional activity of STAT1 increases with a second independent phosphorylation event on S727 (Sadzak et al., 2008). Importantly, when bound to DNA, STAT1 provides transcriptionally competent chromatin through a partnership with histone-modifying enzymes such as the histone acetyltransferase (HAT) CBP, which stimulates gene expression (Wojciak et al., 2009).

We report in this study the identification and characterization of a novel *T. gondii* protein that is exported beyond the parasitophorous vacuole to the host cell nucleus where it interferes with STAT1 dynamics and transcriptional activity. We named it TgIST for “inhibitor of STAT1 transcriptional activity.” We brought compelling evidence that *T. gondii* infection represses IFN- γ -stimulated STAT1-dependent gene expression in a TgIST-dependent manner in both mouse and human cells of different lineages and regardless of parasite strains. Ectopic expression of TgIST in human cells was sufficient to drive the repression of a STAT1-regulated reporter gene, whereas chromatin immunoprecipitation

(ChIP) pointed out the sequestering property of TgIST on STAT1 Y701-P when positioned on the GAS-containing loci. Remarkably, we found that TgIST not only binds to STAT1 Y701-P but also to the chromatin repressor nucleosome remodeling deacetylase (NuRD) complex and corepressor C-terminal-binding protein (CtBP), being thereby ideally positioned to shape the chromatin environment surrounding STAT1-binding sites so as to block IFN- γ -stimulated transcription. Finally, we demonstrated that TgIST avoids early immune-mediated elimination by blocking immunity-related GTPase (IRG)-mediated clearance in macrophages infected by type II persistent parasites.

RESULTS

The ASP5 protease is required for TgIST export into the host cell nucleus

The gene *TGME49_240060* encoding TgIST was originally identified in silico together along with GRA16 (Bougdour et al., 2013) and GRA24 (Braun et al., 2013) in a search for genes encoding parasite effector proteins that are targeted to the host cell nucleus. TgIST is a highly disordered protein that accommodates a transmembrane domain followed by a predicted TEXEL motif (Coffey et al., 2015) and nuclear localization sequences (Fig. 1 A). TgIST protein is unique because it has no significant similarity with any proteins, not even with the close relative *Neospora caninum* proteins. When we monitored TgIST dynamics in *T. gondii* lines expressing the endogenous protein in fusion with the HA-Flag tags, we found that the protein crossed the membrane of mature vacuoles to selectively accumulate in the host cell nucleus (Fig. 1 B). TgIST was detectable in the host cell nucleoplasm as early as 9 h after invasion (Fig. 1 B) and was enriched in the Golgi of the parasites as supported by colocalization with the Golgi marker GRASP (Fig. 1 C). In the absence of the Golgi-resident aspartyl protease ASP5, TgIST was no longer detected in the host cell nucleus (Fig. 1 D), indicating that the protease is essential for TgIST trafficking as it is for GRA16 and GRA24 (Curt-Varesano et al., 2016). Although TgIST-HAFlag was seen by immunoblot analysis as an ~80-kD product when expressed in WT parasites, the protein migrated slightly slower in Δ *asp5* mutant parasites (Fig. 1 E), a situation which would be expected if ASP5 was required for TgIST maturation. Whether the predicted TEXEL motif (Fig. 1 A) corresponds to a direct cleavage site for ASP5 and whether this maturation step is required for TgIST export are yet to be determined.

TgIST binds to STAT1 Y701-P and the chromatin repressor complexes NuRD and CtBPs

To get functional insights on how TgIST traffics to the nucleus, we sought host cell partners by applying Flag affinity chromatography to extracts from primary human foreskin fibroblasts (HFFs) infected with TgIST-HAFlag-expressing tachyzoites. Silver stain analysis of the eluate suggested that TgIST binds to multiple partners under high stringent wash-

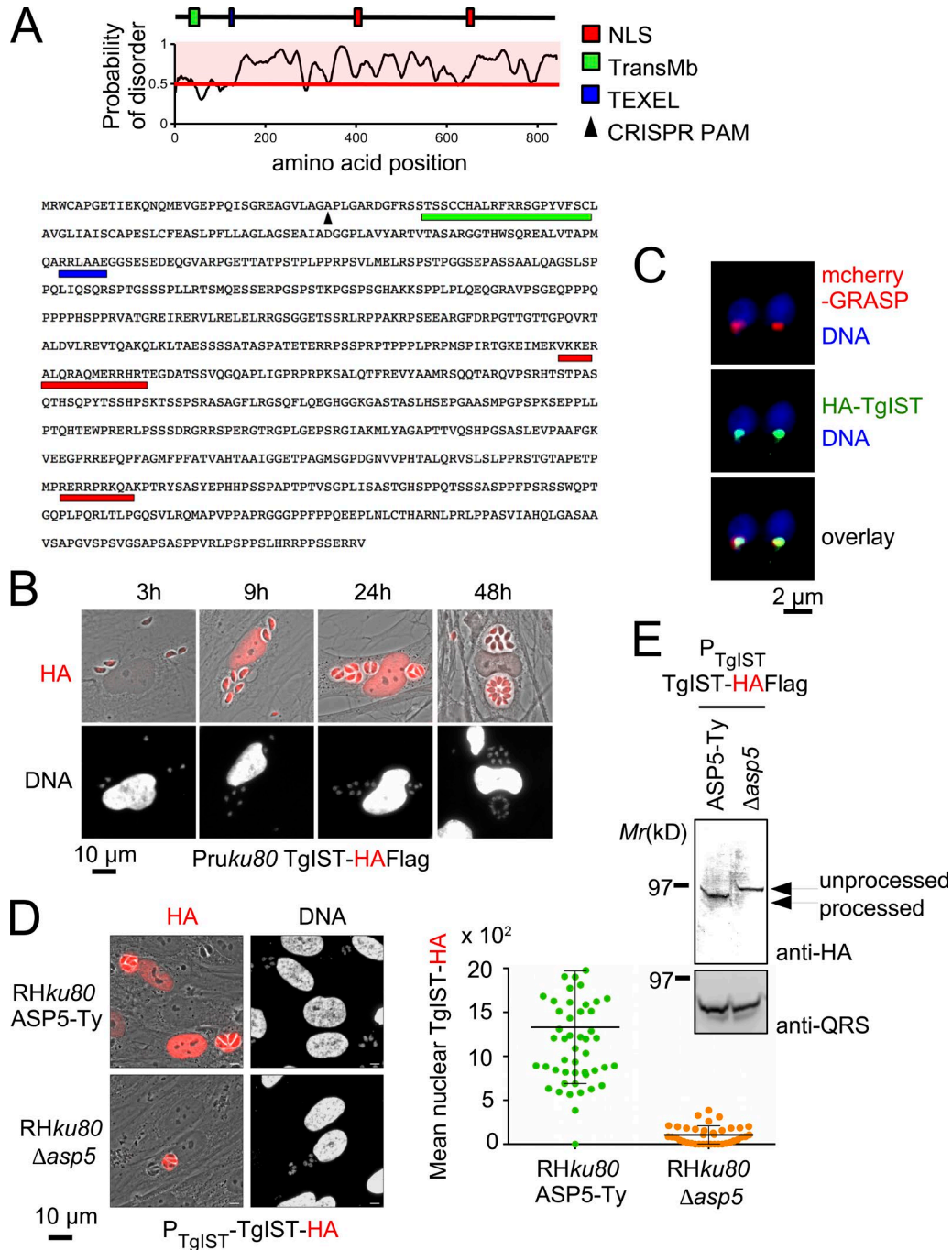


Figure 1. The export of TgIST in the host cell nucleus is mediated by ASP5. (A) Schematic representation of the TgIST protein. Values >0.5 are predicted to be disordered (colored red), and values <0.5 correspond to folded domains. The primary structure of the protein harbors a transmembrane domain (in green) followed by a TEXEL motif (in blue) and two nuclear localization signals (NLS, in red). CRISPR PAM sequence location is indicated (black triangle). (B) Time course of TgIST (HA, in red) secretion and export to the host cell nucleus of HFFs infected with parasites expressing a HAFlag (HF)-tagged copy of TgIST. (C) Colocalization of mCherry-GRASP (in red) and TgIST (HA, in green) at the level of the parasite Golgi after transient expression of the mCherry-GRASP vector in the *Pruk80* TgIST-HAFlag strain. (D) Representative IFA of WT and Δ asp5 parasites transiently expressing P_{TgIST} -TgIST-HAFlag (HA, in red). The amount of TgIST in the nucleus was quantified in at least 50 host cells for each parasite strain. Horizontal bars represent the mean nuclear TgIST intensity \pm SDs. (E) Western blot analysis of extracellular tachyzoites shown in D using anti-HA antibodies. Data are representative of two independent experiments.

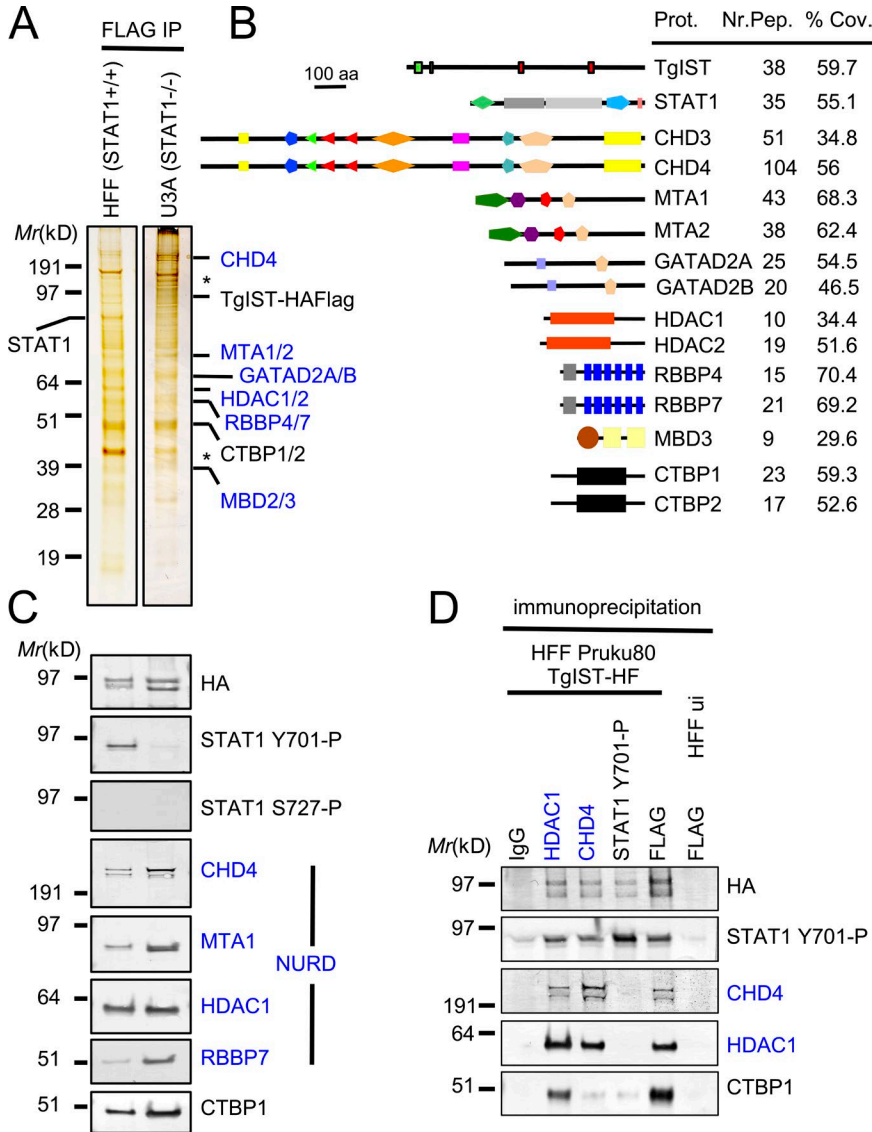


Figure 2. TgIST binds to STAT1 Y701-P and chromatin-bound repressor complexes.

(A) TgIST-associated proteins were purified by Flag chromatography from protein extracts of HFFs and U3A STAT1-deficient cells infected by *Puku80* TgIST-HAFlag. Asterisks indicate degradation products. (A–C) Fractions were analyzed by silver staining (A), mass spectrometry (B), and immunoblotting (C) to detect TgIST-HF (anti-HA) and partners. Identity of the proteins with their respective number of peptides and percentage of coverage are indicated. SMART conserved domains are displayed. NuRD core complex subunits are shown in blue. (D) Coimmunoprecipitation analyses of TgIST-containing complexes. Whole-cell lysates from HFFs left uninfected (ui) or infected with *Puku80* TgIST-HAFlag were immunoprecipitated with the antibodies against the indicated proteins, Flag antibody, and IgG as a negative control. Immunocomplexes were then Western blotted using the indicated antibodies on the right. Data are representative of two independent experiments.

ing conditions (0.5 M NaCl and 0.1% NP-40; Fig. 2 A). These partnerships were subsequently resolved by a combination of mass spectrometry-based proteomics and Western blot analysis that identified TgIST in an intact multisubunit NuRD core complex encompassing chromatin remodeling ATPase (CHD4) and deacetylation (HDAC1,2) enzymes (Fig. 2, B and C; Xue et al., 1998). Additional partners besides NuRD were recognized as the transcriptional corepressors CtBP1 and CtBP2 (Fig. 2, B and C; Chinnadurai, 2002).

Importantly, STAT1 was found in the TgIST-containing eluates under the phosphorylated Y701 status, which promotes the formation of STAT1 homodimer formation, a condition required for STAT1 binding to GAS-containing DNA sequences (Fig. 2, B and C). To determine whether TgIST binding to NuRD or CtBPs depends on STAT1, we repeated the purification scheme using U3A STAT1-deficient cells

(McKendry et al., 1991). The association of TgIST with NuRD and CtBPs was retained in the absence of STAT1 (Fig. 2, A and C). We then validated the interactions by reverse immunoprecipitation using antibodies against NuRD subunits and STAT1 Y701-P (Fig. 2 D) and noticed that STAT1 Y701-P, while displaying a robust binding to TgIST, was not able to pull down the NuRD complex (Fig. 2 D). These data raise the intriguing possibility of a cooperative action between a transcription factor and a chromatin complex coupling lysine deacetylation and ATPase-mediated chromatin remodeling, all factors known to be important for transcriptional repression.

TgIST represses the IFN- γ -mediated STAT1-dependent IRF1 expression

To explore further the role of TgIST in gene repression, particularly in relation to chromatin modification, we analyzed

the influence of the TgIST-containing complex on IRF1 expression because STAT1 is a primary regulator of IRF1 and was previously reported as robustly repressed by *T. gondii* (Kim et al., 2007; Schneider et al., 2013; Rosowski et al., 2014). Infected human and mouse cells did not express IRF1 within 4 h of IFN- γ treatment unlike the neighboring uninfected cells (Fig. 3, A and B). Conversely, IRF1 expression was no longer repressed in cells infected with tachyzoites genetically engineered to lack TgIST (Δ TgIST), thereby indicating that TgIST operates as a transcriptional repressor of *IRF1*. Reintroduction of a copy of TgIST into *TgIST*-deficient parasites resulted in the restoration of IRF1 repression (Fig. 3 C), in agreement with TgIST being necessary and sufficient to regulate IRF1 expression in *T. gondii*-infected cells stimulated with IFN- γ . We then confirmed that TgIST repressor activity occurs at the transcriptional level (Fig. 3 D). Finally, although nuclear accumulation of TgIST was retained in the absence of STAT1 (Fig. 3 E, left), IFN- γ treatment was inefficient at driving IRF1 expression in STAT1-deficient U3A cells regardless of the infection status (Fig. 3 E, right), highlighting the importance of STAT1 in the control loop of IRF1 transcription.

***T. gondii* genome-wide alteration of STAT1-dependent transcription is mediated by TgIST**

The ability of TgIST to repress IRF1 expression prompted us to investigate whether the parasite protein could regulate IFN- γ -induced gene expression in a broader fashion. To this end, we first performed a genome-wide expression profiling of HFFs left uninfected or infected for 24 h with 76KGFP (WT) and 76KGFP Δ TgIST (Δ) and stimulated 6 h with IFN- γ (Fig. 4 A). We focused our analysis on genes displaying more than a fourfold change when comparing the Δ TgIST mutant with the parental strain. Gene set enrichment analysis (GSEA) highlighted seven pathways significantly and selectively repressed ($P < 0.05$) in a TgIST-dependent fashion (Fig. 4 B). A majority of these pathways clustered into biological processes related to immunity, including signaling through NF- κ B and those involved in IFN- γ response (Fig. 4 B). Indeed, many inflammatory genes can be synergistically up-regulated by both the STAT1/IRF1 and NF- κ B transcription factors because their promoters contain transcription factor binding sites (TFBSs) for both STAT1 and NF- κ B. Quantitative RT-PCR of the mRNA levels of six secondary IFN- γ response genes (CXCL9, CXCL10, CIITA, MX1, GBP2, and IGTP) revealed a similar profile with a repression of gene expression triggered by infection with WT parasites but not with TgIST-deficient tachyzoites (Fig. 4, C and D), which presumably reflects the lack of both STAT1 and IRF1 for their transcriptional activation.

To evaluate the contribution of STAT1 to the TgIST-mediated repression of IFN- γ -induced genes, we performed a comprehensive profiling of gene expression in STAT1-null U3A versus parental 2fTGH cells first infected either by WT or Δ TgIST parasites and then stimulated by

IFN- γ . 234 unique genes were at least fourfold regulated in *T. gondii*-infected IFN- γ -stimulated cells in a TgIST-dependent manner when comparing 2fTGH with U3A cells (data are accessible through NCBI GEO accession no. GSE81613). Hierarchical clustering of the 70 top-ranked genes (more than fourfold, false discovery rate $< 1\%$) delineated clusters of coregulated IFN- γ -induced transcripts that are repressed by *T. gondii* infection in both a TgIST- and STAT1-dependent manner (Fig. 5 A). Analysis of regulatory elements of these genes revealed enrichment of IRF1 and STAT1 (ISRE) TFBSs in their promoters (Fig. 5, B and C). GSEA hallmark analysis highlighted that gene products belonging to IFN- γ - and IFN- α -related pathways were highly enriched (Fig. 5 D). These data suggested that beyond negatively regulating IRF1 (Fig. 3), TgIST contributes more widely to inhibit IFN- γ -mediated STAT1-dependent gene regulation.

Ectopic expression of TgIST is sufficient to repress STAT1-dependent promoter

We next wanted to determine whether TgIST alone was sufficient to repress STAT1-dependent promoter or whether other *T. gondii* effectors might contribute to the phenotype. Therefore, we constructed mammalian expression vectors carrying N- or C-terminal epitope-tagged TgIST to monitor TgIST activity in HEK-Blue IFN- γ sensor cells. These cells express a fully active STAT1 signaling pathway and a reporter gene under the control of an ISG54 promoter fused to four GAS elements. We first confirmed that, regardless of the tag position, TgIST chimeric proteins were similarly targeted to the host cell nucleus (Fig. 6 A and not depicted) as when delivered by intracellular parasites and second that TgIST expression significantly repressed (approximately threefold) the expression of the reporter gene by IFN- γ (Fig. 6 B). These data are consistent with TgIST being sufficient to control STAT1 activity.

TgIST modulates the phosphorylation status of STAT1

To get insights on the mechanism by which TgIST regulates STAT1 activity, we examined whether infection and IFN- γ stimulation modified the phosphorylation status and cellular location of STAT1 isoforms. Immunoblot analysis of cytoplasmic and nuclear fractions revealed that inactive STAT1 localized mainly in the cytoplasm of resting cells (Fig. 6 C, lane 1) and underwent a transient phosphorylation on Y701, an event which concurred with nuclear localization in IFN- γ -stimulated cell (Fig. 6 C, compare lanes 2 and 4). Active STAT1 Y701-P, in turn, fostered transcriptional activation of primary IFN- γ response genes such as *IRF1* (Fig. 6 C, lane 4). After infection, we observed a drastic change in the subcellular localization of the STAT1 isoforms. In the absence of IFN- γ stimulation, infected cells harbored a genuine signature of a fully active STAT1 (STAT1 Y701-P), but intriguingly, the protein remained transcriptionally incompetent as no IRF1 protein was detected (Fig. 6 C, lanes 5 and 6). In the presence of IFN- γ , the expression levels of IRF1

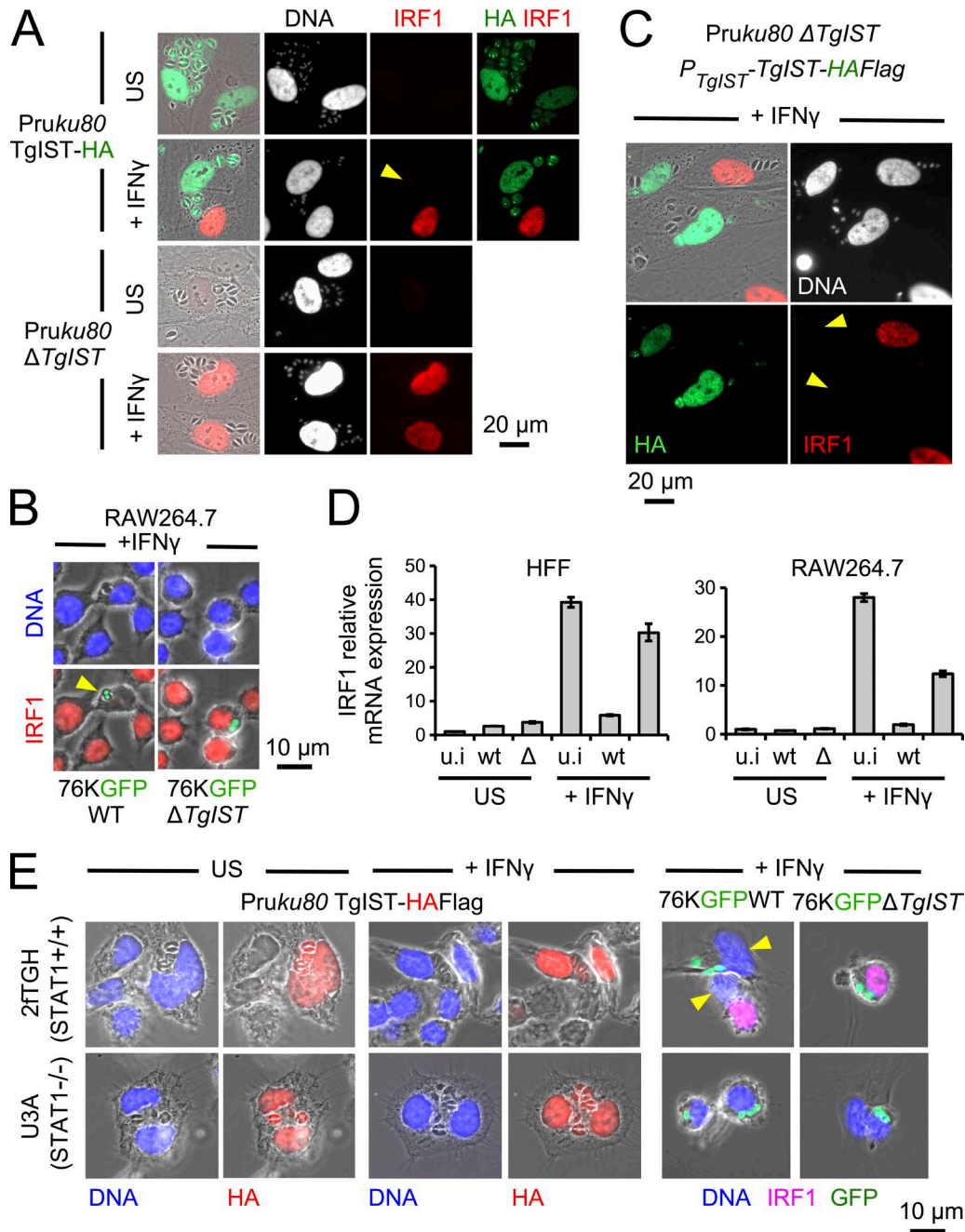


Figure 3. **TgIST is required to inhibit IFN- γ -induced IRF1 expression.** (A) HFFs were infected for 24 h with *Pruku80* TgIST-HAFlag or *Pruku80* Δ TgIST and stimulated 6 h with IFN- γ or left unstimulated (US). Cells were stained to detect nuclear localization of IRF1 (red) and TgIST (HA, green). (B) IFN- γ -induced IRF1 expression was monitored in mouse macrophages as described in A after infection with 76KGFP-WT and Δ TgIST. GFP-expressing parasites (green) and IRF1 (red) were detected. (C) HFFs were infected for 24 h with Δ TgIST parasites transiently expressing a copy of P_{TgIST} -TgIST-HAFlag whose expression was driven by its own promoter. After IFN- γ stimulation, TgIST (HA, green) and IRF1 expression (red) were detected. (D) *IRF1* mRNA levels were determined by RT-qPCR in both HFFs and RAW264.7 infected and stimulated as described in A. *β 2-microglobulin* was used for normalization. Data are displayed as fold difference relative to the uninfected cells. The mean of two experiments is shown; error bars represent SEM. This was performed three times with similar results. (E, left) Export of TgIST (HA, red) in U3A STAT1-deficient cells and the corresponding parental line 2fTGH. Cells were infected for 24 h with *Pruku80* TgIST-HAFlag and stimulated 6 h with IFN- γ or left unstimulated (US). (right) IFN- γ -induced IRF1 expression (magenta) was monitored in 2fTGH and U3A infected for 24 h with 76KGFP-WT and Δ TgIST and stimulated for 6 h with IFN- γ . Immunofluorescence data are representative of at least three experiments. Yellow arrowheads indicate infected cells in which IRF1 expression was repressed.

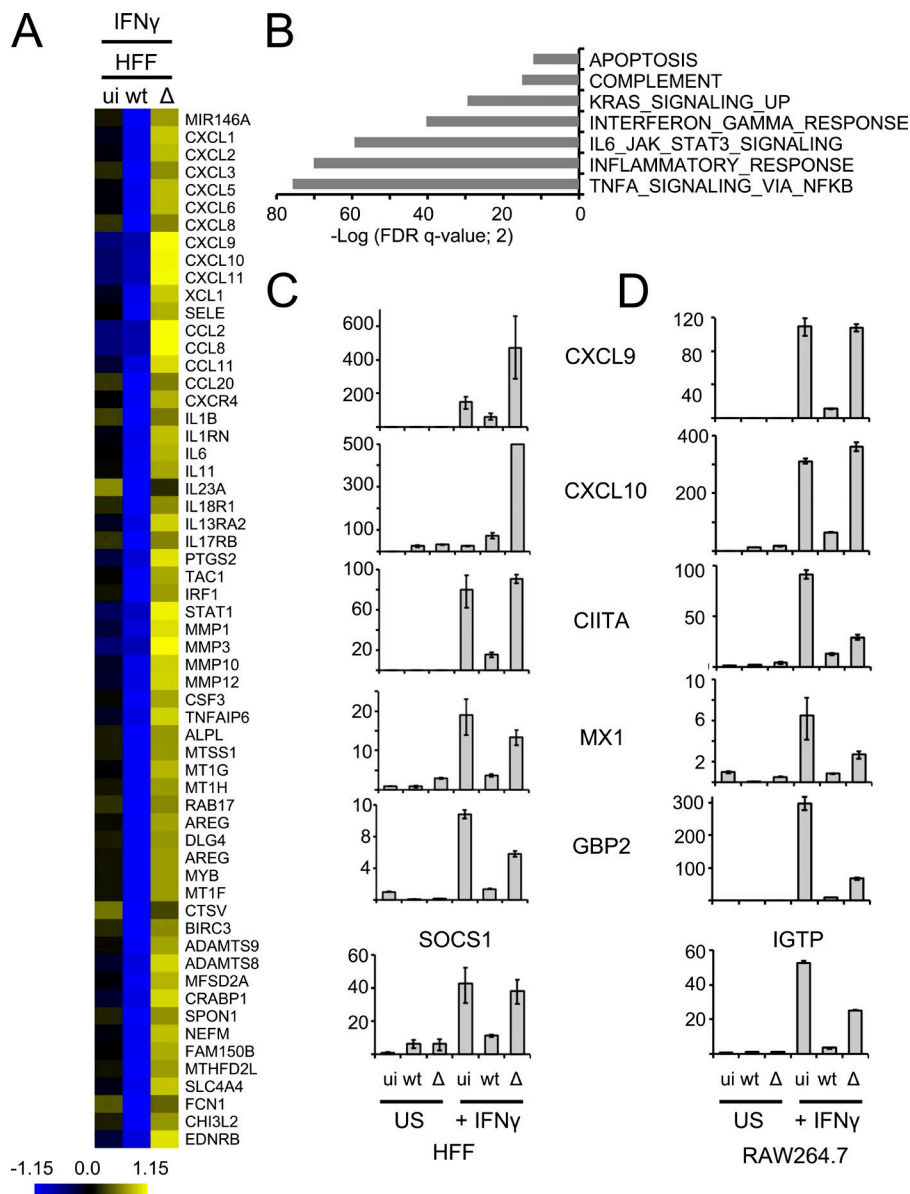


Figure 4. *T. gondii* inhibits IFN- γ -induced gene expression in a TgIST-dependent fashion. (A) TgIST represses IFN- γ -induced genes in human fibroblasts. HFFs were infected for 24 h with 76KGF (WT) and 76KGF Δ TgIST (Δ) or left uninfected (ui) and stimulated 6 h with IFN- γ . Heat map of expression values for the 60 most differentially expressed genes between WT and Δ TgIST. Mean log₂ gene expression values were median centered, and genes were clustered according to the biological pathways identified. The complete set of genes is listed in the GEO dataset (accession no. GSE81613). (B) Top-scoring pathways regulated by TgIST in a STAT1-dependent manner and upon IFN- γ stimulation in HFFs were determined by GSEA. (C and D) Human and mouse cells were infected for 24 h with Pruku80 (WT) and Pruku80 Δ TgIST (Δ) or left uninfected (ui) and stimulated for 6 h with IFN- γ or left unstimulated (US). Levels of CXCL9, CXCL10, CII TA, MX1, GBP2, IGTP, and SOCS1 mRNAs were determined by RT-qPCR. β 2-microglobulin was used for normalization. Data are displayed as fold difference relative to the uninfected cells. The mean of two experiments is shown; error bars represent SEM. This experiment is representative of at least three experiments and was repeated with 76KGF (WT and Δ) strains with similar results (not depicted).

in cells infected with WT parasites were kept lower than in uninfected cells (Fig. 6 C, compare lanes 4 and 8), in line with the repressor activity of TgIST seen at the transcriptional level (Fig. 3 D). When cells were infected with Δ TgIST tachyzoites, none of the effects induced by WT parasites were observed as the distribution of STAT1 isoforms or the level of IRF1 expression recapitulated those of uninfected cells independently of IFN- γ treatment, thus stressing the pivotal role of TgIST in driving the responses to IFN- γ (Fig. 6 C, lanes 9–12). We also observed that infection of unstimulated cells promoted the phosphorylation of S727 in a TgIST-dependent fashion (Fig. 6 C, compare lanes 6 and 10). Originally, S727 phosphorylation of STAT1 was shown to occur exclusively after the stable association of STAT1 Y701-P with chromatin at the vicinity of IFN- γ -inducible genes (Sadzak et al.,

2008). Finally, we found the subcellular distribution of both all NuRD subunits and CtBP1 to be unaltered upon infection (Fig. 6 C). We concluded from these data that the TgIST repressor effect on STAT1 activity coincided with phosphorylation of STAT1, a modification that could increase STAT1 ability to associate with chromatin.

TgIST enhances occupancy of fully activated STAT1 on GAS-containing loci

Because STAT1 Y701-P was markedly enriched in the nucleus of cells infected by *T. gondii*, we hypothesized that TgIST could interfere with STAT1 function at the chromatin level. To test whether TgIST affected STAT1 binding to chromatin, we performed ChIP analysis on samples probed across the *IRF1* locus and found that in the absence of IFN- γ

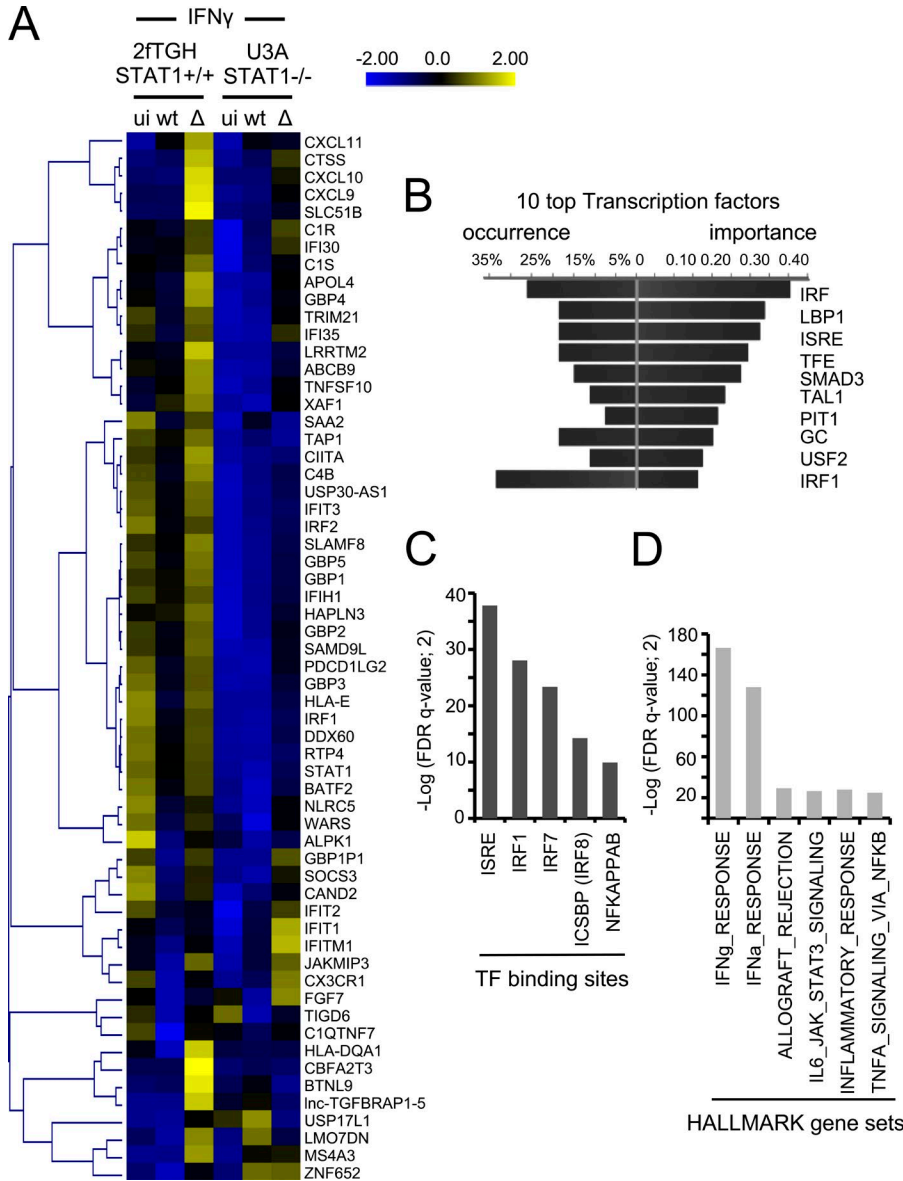


Figure 5. **TgIST represses IFN- γ -induced gene expression in human epithelial cells in a STAT1-dependent manner.** (A) Heat map of expression values for differentially expressed genes in U3A versus 2fTGH cells infected with 76KGF (WT) or $\Delta TgIST$ (Δ) parasites. For the 70 genes that are defined as core TgIST- and STAT1-regulated genes, mean log₂ gene expression values were median centered, genes were clustered by hierarchical clustering, and a heat map is presented. The complete set of genes is listed in GEO dataset (accession no. GSE81613). (B and C) TFBS analysis of STAT1-regulated core genes influenced by TgIST was performed by DIRE (B) and GSEA (C), and the most significant transcription factors (TF) are listed. (D) Top-scoring pathways regulated by TgIST in a STAT1-dependent manner and upon IFN- γ stimulation were determined by GSEA.

stimulation, STAT1 Y701-P was enriched at the *IRF1*-GAS in a TgIST-dependent manner (Fig. 7 A, compare bars 1, 3, and 5). Because IFN- γ treatment induced a STAT1 recruitment we found to be exacerbated by WT but not *TgIST*-deficient tachyzoites (Fig. 7 A, compare bars 2, 4, and 6), we next hypothesized that TgIST prolongs STAT1 occupancy at the chromatin, a sequestering activity that would account for the slow STAT1 recycling to the cytoplasm. Of note, the dual Y701-S727 phosphorylation of STAT1 is known to characterize the chromatin-bound pool of STAT1 (Sadzak et al., 2008), and we observed this STAT1 (Y701/S727)-P isoform to be significantly enriched at the *IRF1*-GAS location in particular in the presence of WT parasites (Fig. 7 A). Next, when we analyzed the STAT1 isoforms present at the chromatin, both Y701-P and S727-P forms persisted at the chromatin near the GAS-driven secondary genes (i.e., *CXCL10* and *CII*

TA; Fig. 7 B, and C). We concluded that the TgIST inhibitory activity on STAT1 involves the stable association of STAT1 with the promoter region of the IFN- γ -regulated genes in a way that protects the DNA-bound STAT1 molecules from dephosphorylation while promoting S727 phosphorylation.

TgIST remodels the chromatin environment at the STAT1-binding site

STAT1 sequestration at the chromatin does not explain the mechanism underlying transcriptional repression by TgIST of *IRF1* expression. We thus next asked whether the deacetylase activity of the TgIST-associated HDAC1 and 2, previously identified as interacting with TgIST (Fig. 2), could account for the transcriptional repression activity of TgIST. In agreement with a previous study (Rosowski et al., 2014), we showed that treatment of infected cells with HDAC inhibitors

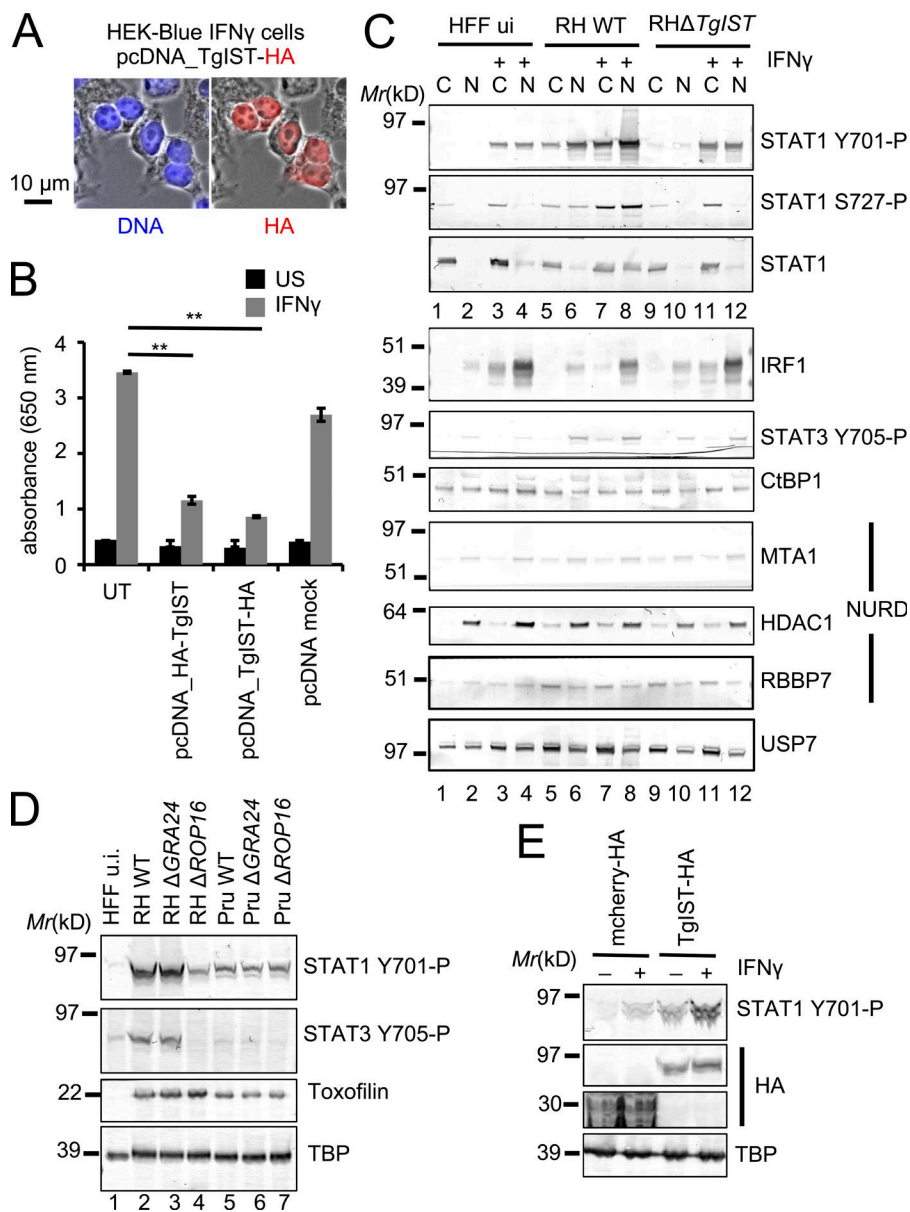


Figure 6. TgIST represses GAS-containing loci by enhancing occupancy of activated STAT1 at DNA. (A and B) HEK-Blue IFN- γ sensor cells expressing an active STAT1 signaling pathway were transfected with pcDNA_HA-TgIST, pcDNA_TgIST-HA, or pcDNA mock or left untransfected (UT) and stimulated 24 h with IFN- γ or left unstimulated (US). (A) Nuclear localization of TgIST-HA (in red) was confirmed. (B) Cell supernatant for each aforementioned condition was collected and tested for the presence of reporter gene SEAP. Error bars represent the SD calculated from results of three independent experiments. **, $P < 0.005$ (Student's t test). (C) Cellular fractionation of HFFs infected 24 h by WT or Δ TgIST or left uninfected (ui) and stimulated 6 h with IFN- γ or left unstimulated. Cytosolic (C) and nuclear (N) cell lysates were probed with the indicated antibodies. USP7 levels are shown as loading control. This experiment is representative of two experiments and was repeated with *Pruku80* (WT and Δ) strains with similar results (not depicted). (D) Immunoblotting detection of STAT1 Y701-P and STAT3 Y705-P in unstimulated HFFs left uninfected (u.i.) or infected 24 h with type I RH*ku80* (WT) or type II *Pruku80* (WT) and their corresponding Δ *gra24* and Δ *rop16* mutants. TBP (host specific) and Toxofilin (parasite specific) levels are shown as loading controls. (E) RAW264.7 cells were transfected with pcDNA_TgIST-HA or mock pcDNA_mcherry-HA and stimulated 24 h with IFN- γ or left unstimulated. Ectopic expression of both TgIST and mcherry (HA) and the levels of STAT1 Y701-P were determined by immunoblotting. TBP levels are shown as loading control. The experiments were repeated two times.

(HDACs) targeting both class I and II enzymes did not prevent TgIST from inhibiting IFN- γ -induced expression of IRF1 (not depicted). Likewise, we confirmed that the levels of three major histone acetylated marks (i.e., H3K9ac, H3K27ac, and H4K5,8,12,16ac) remained unchanged at STAT1-binding loci after infection (Fig. 7 D). Although counterintuitive, the lack of hypoacetylation of neighboring nucleosomes at GAS-containing loci (Fig. 7 D) in the presence of a direct interaction between HDAC1,2 enzymes and TgIST (Fig. 2) can also be explained by a competition between HDAC and HAT that would dynamically regulate STAT1 acetylation (Krämer and Heinzel, 2010).

To investigate further the chromatin contribution to TgIST-mediated gene repression, we next analyzed whether other histone modifications could be found across the *IRF1*

gene locus. We chose to track the H3K4me1/me3 histone modifications because they were reported as a genome-wide signature for STAT1-binding sites in HeLa cells (Robertson et al., 2008). We found that H3K4me3 was significantly enriched (\sim 20-fold) with *IRF1*-GAS in resting cells but was quasi-absent from this promoter region and instead drastically increased at the middle region of the gene (\sim 70-fold) upon IFN- γ stimulation (Fig. 7 A, compare bars 1, 2, 7, and 8), an observation consistent with ongoing transcription (Fig. 3 D). Infection with WT but not with Δ TgIST tachyzoites led to a marked increase of H3K4me3 levels at the promoter, which was potentiated by IFN- γ to reach a 60-fold enrichment (Fig. 7 A, bars 3–6). Importantly, depletion of the histone mark into the coding region that followed IFN- γ treatment (Fig. 7 A, compare bars 8 and 10) correlated with the

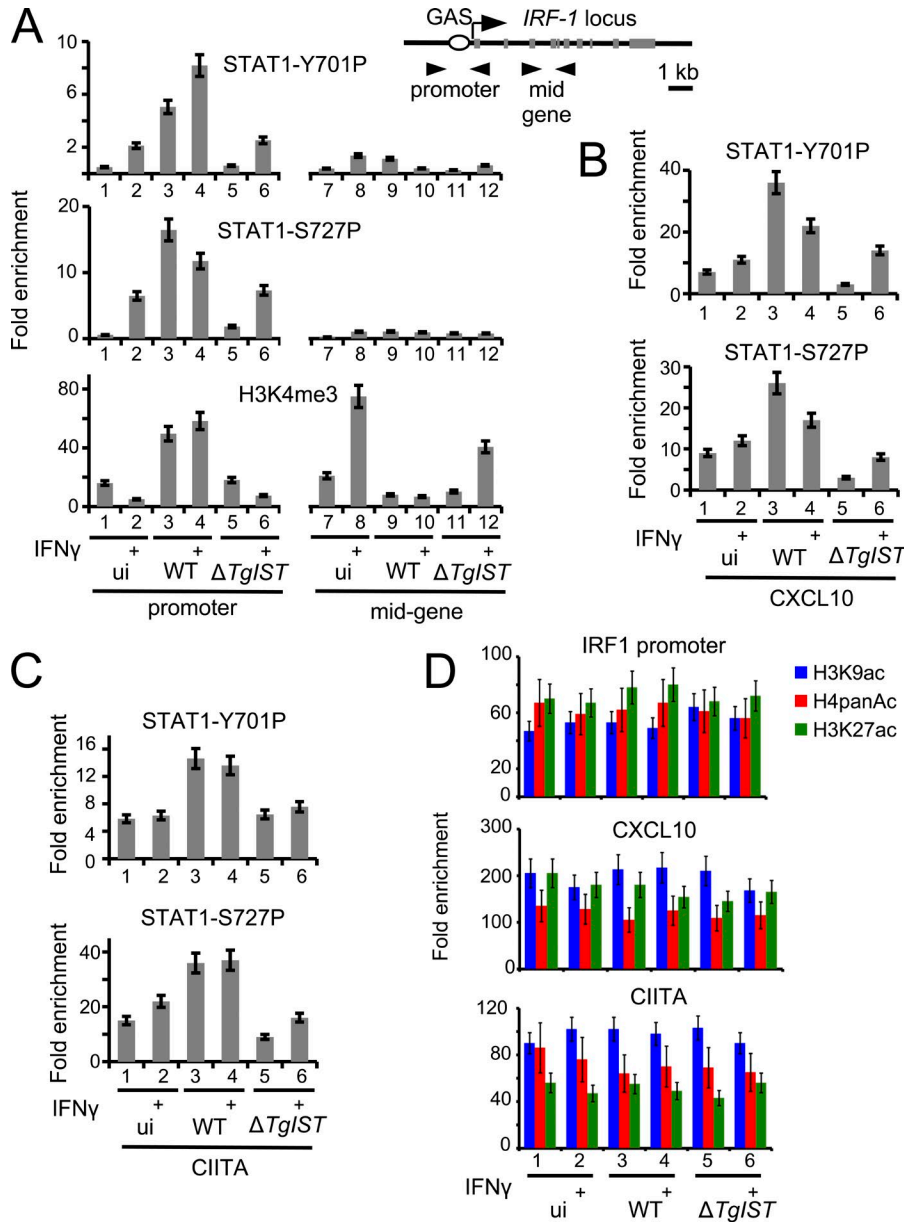


Figure 7. IFN- γ -induced activated STAT1 DNA association is enhanced by *T. gondii* in a TgIST-dependent manner. (A–C) HFFs were infected for 24 h with *Pruku80* (WT) and *Pruku80* Δ TgIST (Δ TgIST) or left uninfected (ui) and stimulated 6 h with IFN- γ (+) or left unstimulated. Samples were analyzed by ChIP assay with antibodies to STAT1 Y701-P, STAT1 S727-P, and H3K4me3. IgG was used as negative control. Bound DNA corresponding to IRF1, CXCL10, and CIITA loci was quantified by qPCR-ChIP, and signals were normalized with the input DNA. Error bars represent SD ($n = 3$). Data are from one representative of three independent experiments. (D) ChIP-qPCR was used as aforementioned to monitor enrichment of H3K9ac, H4panAc, and H3K27ac at IRF1, CXCL10, and CIITA promoters. Error bars represent SD ($n = 3$). Data are from one representative of two independent experiments.

TgIST-mediated repressed state of *IRF1* (Fig. 3 D). Because H3K4me3 marks active promoters, its pattern and dynamics after infection at the *IRF1* locus are reminiscent of bivalent chromatin domains capable of silencing developmental genes while keeping them poised for rapid activation (Voigt et al., 2013; Matsumura et al., 2015).

The IRG load on the parasitophorous vacuoles was increased for Δ TgIST parasites together with the increased parasite clearance in IFN- γ -activated macrophages

A major defense mechanism of innate immunity against *T. gondii* is mediated by the IFN- γ -inducible IRG pathway (Collazo et al., 2002; Howard et al., 2011). Given that TgIST interferes with the IFN- γ -STAT1 pathway, we tested

whether TgIST could affect IRG expression and/or activity. IRGs are cytoplasmic proteins that target and disrupt the young parasitophorous vacuole membrane (PVM) surrounding type II avirulent but not type I virulent *T. gondii* strains, the latter being able to counteract IRG function through the kinase activity of secreted ROP5/ROP18/ROP17 products (Martens et al., 2005; Etheridge et al., 2014). We first examined Irgb6 in IFN- γ -prestimulated mouse cells and detected similar high enrichment of Irgb6 at the PVM of either WT or TgIST-deficient type II tachyzoites (Fig. 8 A, top). In sharp contrast, when cells were infected first and then stimulated with IFN- γ , the PVM of WT type II parasites showed lower Irgb6 loading than those of TgIST mutant strain (Fig. 8 A, bottom), consistent with the early TgIST-mediated repression

at the transcriptional level before IFN- γ trigger. As previously reported, type I parasites prevented the *Irgb6* loading (Zhao et al., 2009); *Irgb6* loading was not significantly affected by the absence of *TgIST* (Fig. 8 B), very likely because of the ROP5/ROP18-mediated IRG inactivation. These data suggest that ROP5/ROP18 are epistatic to *TgIST* function in the IFN- γ pathway and bring strong evidence that *T. gondii* infection regulates at the transcriptional level *Irgb6* expression in a *TgIST*-dependent manner (Fig. 8 C).

In these assays we also assessed parasite growth. Considering the known activity of *Irgb6* loading on the PVM disruption, it was not surprising to observe a decrease (twofold) in parasite growth in the absence of *TgIST* when BMDM or RAW264.7 cells were infected before IFN- γ (Fig. 8, D and E). However, we saw that when cells were prestimulated with IFN- γ before infection, growth of both WT and *TgIST* mutant type II parasites was inhibited, very likely as the result of *TgIST* failing to inhibit transcription once host cell effector proteins were produced (Fig. 8 D and not depicted).

Influx of Gr1⁺ inflammatory monocytes associates with the limited expansion of *TgIST*-deficient parasites in mice

Because IFN- γ -dependent effector mechanisms are critical for the control of the *T. gondii* burden in mice and because *TgIST* was shown to regulate IFN- γ -mediated responses, we compared the parasitic process in BALB/c inbred mice after i.p. injection of either WT or *TgIST*-deficient parasites expressing luciferase, the inoculum content ranging from 5×10^4 to 5×10^5 tachyzoites. Monitoring parasite multiplication and dissemination with in vivo bioluminescent imaging, we found a reduction in the $\Delta TgIST$ parasite population size when compared with the WT population that started as early as day 5 postinfection (p.i.) and that markedly rose up with time over the 9 d of assay (Fig. 9 A). In line with the bioluminescence analysis, mice inoculated with a lethal dose (5×10^5) of WT failed to establish a chronic infection and died within 6 d p.i., whereas mice infected with the same dose of $\Delta TgIST$ showed a 60% survival (Fig. 9 B). We next quantified parasites recovered from the peritoneal cavity after injection of higher dose of tachyzoites (10^5) and confirmed the rapid control of the $\Delta TgIST$ population when compared with WT parasites using parasite DNA quantification by real-time PCR (Fig. 9 C) or GFP-based detection of the tachyzoites (Fig. 10 A).

To investigate whether *TgIST* contributes to the early innate events that determine the priming of adaptive immunity, we measured local (peritoneal fluid, Fig. 9 C) and systemic (plasma, not depicted) cytokine profiles over time, after infection. From day 7 to day 9 p.i., we observed that mice infected with *TgIST*-deficient parasites produced significantly less of the “late” proinflammatory IFN- γ , IL-6, IL-1 β , and IL-18 cytokines and antiinflammatory IL-10 cytokine in their peritoneal cavities than mice infected with the parental strain (Fig. 9 C). In contrast, the early source of IL-12 driving protective Th1 responses to *T. gondii* remained unchanged

from days 5 to 9 (Fig. 9 C). Thus, *TgIST*-deficient parasites, although still efficient to mount a proper Th1 response, were unsuccessful to expand in vivo. We also assessed whether a potent cellular response could account for the early control of the $\Delta TgIST$ parasite population. Previous studies have emphasized the critical role of inflammatory Gr1⁺ monocytes inflowing at the *T. gondii* infection site to control acute toxoplasmosis in mice (Robben et al., 2005; Dunay et al., 2008). In this regard, we examined by FACS whether the control of *TgIST*-deficient parasites could be assigned to differences in the early cellular recruitment of myeloid cells in the peritoneal cavity. After i.p. inoculation of BALB/c mice with a high dose of tachyzoites (10^5), resident peritoneal monocytes (CD11b⁺ Gr1⁻ Ly6G⁻) were gradually replaced by both neutrophils (CD11b⁺ Gr1^{high} Ly6G⁺) and activated inflammatory monocytes (CD11b⁺ Gr1^{int} Ly6G⁻; Fig. 10, B and C). Of note, a significant gap was first detected at day 7 p.i. in the relative and absolute amounts of inflammatory monocytes between mice infected with WT or *TgIST*-deficient parasites (Fig. 10, B and C). Therefore, homing of the CD11b⁺ Gr1^{int} Ly6G⁻ cells is likely to play a pivotal role in the control of *TgIST*-deficient parasite expansion (Figs. 9 A and 10 A).

DISCUSSION

T. gondii elicits a strong Th1 inflammatory response typified by the secretion of substantial levels of IFN- γ by CD4⁺, CD8⁺ T lymphocytes and NK cells in both humans and mice (Sturge and Yarovinsky, 2014; Yarovinsky, 2014). IFN- γ drives the expression in infected cells of multiple antimicrobial proteins that are instrumental in activating cell-autonomous immunity against intracellular *T. gondii*. In mice, the two major IFN- γ -induced protein families, i.e., IRGs and guanylate-binding proteins (GBPs), actively cooperate to target parasites that reside in parasitophorous vacuoles by inducing PVM disruption (Martens et al., 2005; Zhao et al., 2009; Yamamoto et al., 2012), whereas GBPs can in addition attack the parasite membrane (Kravets et al., 2016). Although these immune effectors transform the infected cell into a hostile environment and account for the restriction of avirulent type II *T. gondii* populations, their action is expected and partially counteracted, hence allowing the persistence of type II strains in animals.

Early studies have reported that *T. gondii* counter-defense remodels the host cell to be unresponsive to IFN- γ at the transcriptional level in both humans and mice (Zimmermann et al., 2006; Kim et al., 2007; Lang et al., 2012). Next, it was convincingly argued that *T. gondii* infection inhibits STAT1 transcriptional activity by preventing its nuclear-cytoplasmic cycling (Rosowski et al., 2014); however, the identity of the parasite effector remained unknown. In this study, we identified the missing link as *TgIST* and we uncovered how *TgIST* down-regulates IFN- γ -dependent signaling. Although this STAT1 silencing device appeared beneficial to the early phase of *T. gondii* infection by protecting the first wave of invading tachyzoites from the potent antiparasitic

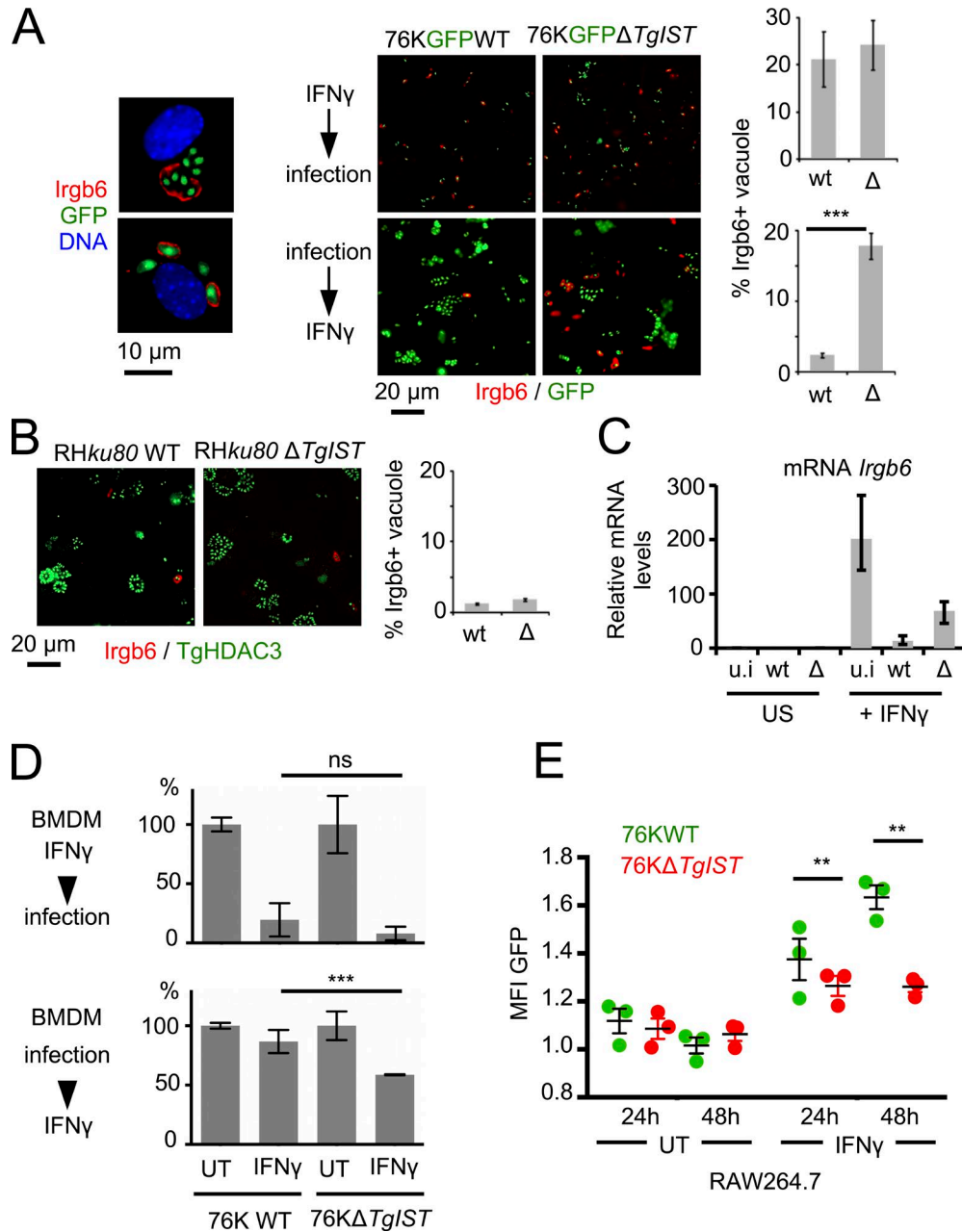


Figure 8. Δ *TgIST*-containing vacuoles display increased IRG loading and are more sensitive to clearance in macrophages when cells are IFN- γ stimulated after infection. (A) In the top panel, mouse tail fibroblasts were stimulated 18 h with IFN- γ before infection for 4 h with type II 76KGFP (WT) and 76KGFP Δ *TgIST* (Δ) strains. In the lower panel, mouse tail fibroblasts were infected for 4 h and then stimulated 12 h with IFN- γ . IFA with Irgb6 (red) at the PVM was quantified. Enlarged fields of Irgb6 loading at the PVM are shown on the left. Means \pm SEM; $n = 3$ samples each from three combined experiments. ***, $P < 0.005$ (Student's t test). Data are from one representative of two independent experiments. (B) Mouse tail fibroblasts were infected for 4 h with type I RHku80 (WT) and RHku80 Δ *TgIST* (Δ) strains and then stimulated 12 h with IFN- γ . TgHDAC3 (green) and Irgb6 (red) were detected by IFA, and the loading of Irgb6 at the PVM was quantified. Means \pm SEM; $n = 3$ samples each from three combined experiments. (C) *Irgb6* mRNA levels were determined by RT-qPCR in mouse tail fibroblasts left uninfected (u.i.) or infected with 76KGFP strain (WT) and 76KGFP Δ *TgIST* (Δ) and then stimulated with IFN- γ . β 2-microglobulin was used for normalization. Data are displayed as fold difference relative to the uninfected cells. The mean of two experiments is shown; error bars represent SEM. This was performed two times with similar results. (D) In vitro clearance of parasites in mouse BMDMs that were prestimulated (12 h) before infection (36 h; top graph) or infected (8 h) and then stimulated (40 h; bottom graph). Type II 76KGFP strain (WT) and 76KGFP Δ *TgIST* (Δ) were used for infection. Parasite growth was evaluated by high-content imaging assay using the scanR system (Olympus). Means \pm SEM. ***, $P < 0.005$ (Student's t test). (E) In vitro clearance of parasites in RAW264.7 mouse macrophages that were infected for 12 h with type II 76KGFP (WT) and 76KGFP Δ *TgIST* (Δ) strains and then stimulated with IFN- γ for 24 or 48 h or left unstimulated (UT). The MFI of GFP expression was quantified by flow cytometry. Means \pm SEM; $n = 3$ combined independent experiments. **, $P \leq 0.0354$ (two-way ANOVA test).

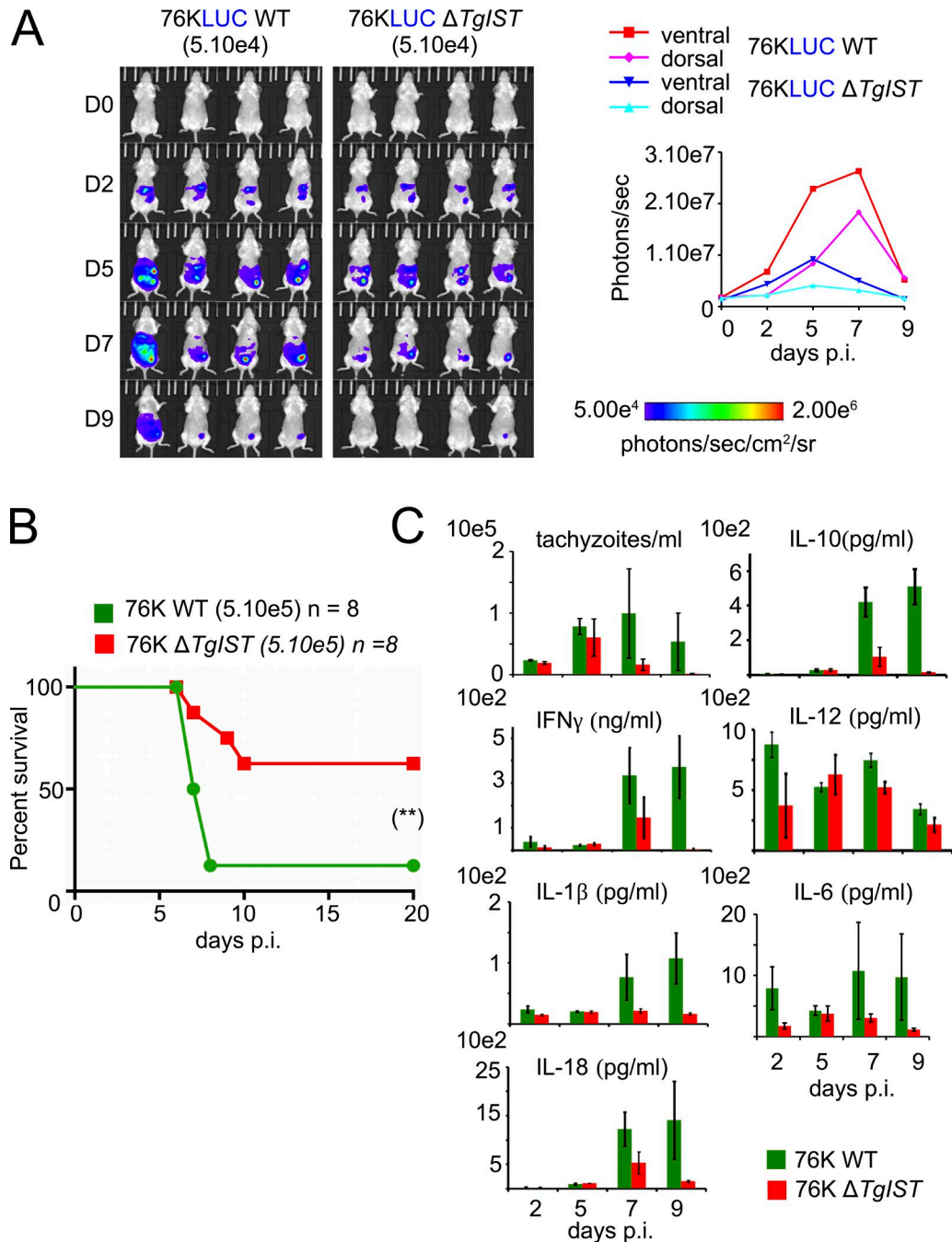


Figure 9. **Control of *TgIST*-deficient parasite expansion in vivo is associated with an efficient Th1 response.** (A) Luminescent parasites were imaged with an IVIS imaging system from day 0 to 9 after the i.p. inoculation to BALB/c of 5.10^4 tachyzoites per condition. Graph on the right depicts mean whole-animal radiance. (B) Virulence of $\Delta TgIST$ strain was compared with its parental 76K GFP in BALB/c mice. Mice ($n = 8$) were inoculated with 5×10^5 tachyzoites by i.p. injection, and survival was monitored. Significance was tested using Log-rank (Mantel-Cox) test (**, p -value = 0.0161) and Gehan-Breslow-Wilcoxon test (**, p -value = 0.0154). (C) BALB/c mice were given i.p. a dose of 10^5 76KLUC-WT or 76KLUC $\Delta TgIST$ tachyzoites. Peritoneal lavage fluids were collected on days 2, 5, 7, and 9 after inoculation. Number of tachyzoites was estimated within the collected samples by parasite DNA PCR and concentrations of IL-1 β , IL-6, IL-10, IL-12, IL-18, and IFN- γ were determined by ELISA. Data shown are means \pm SD with $n = 3$ individual mice per parasite genotype at each time point.

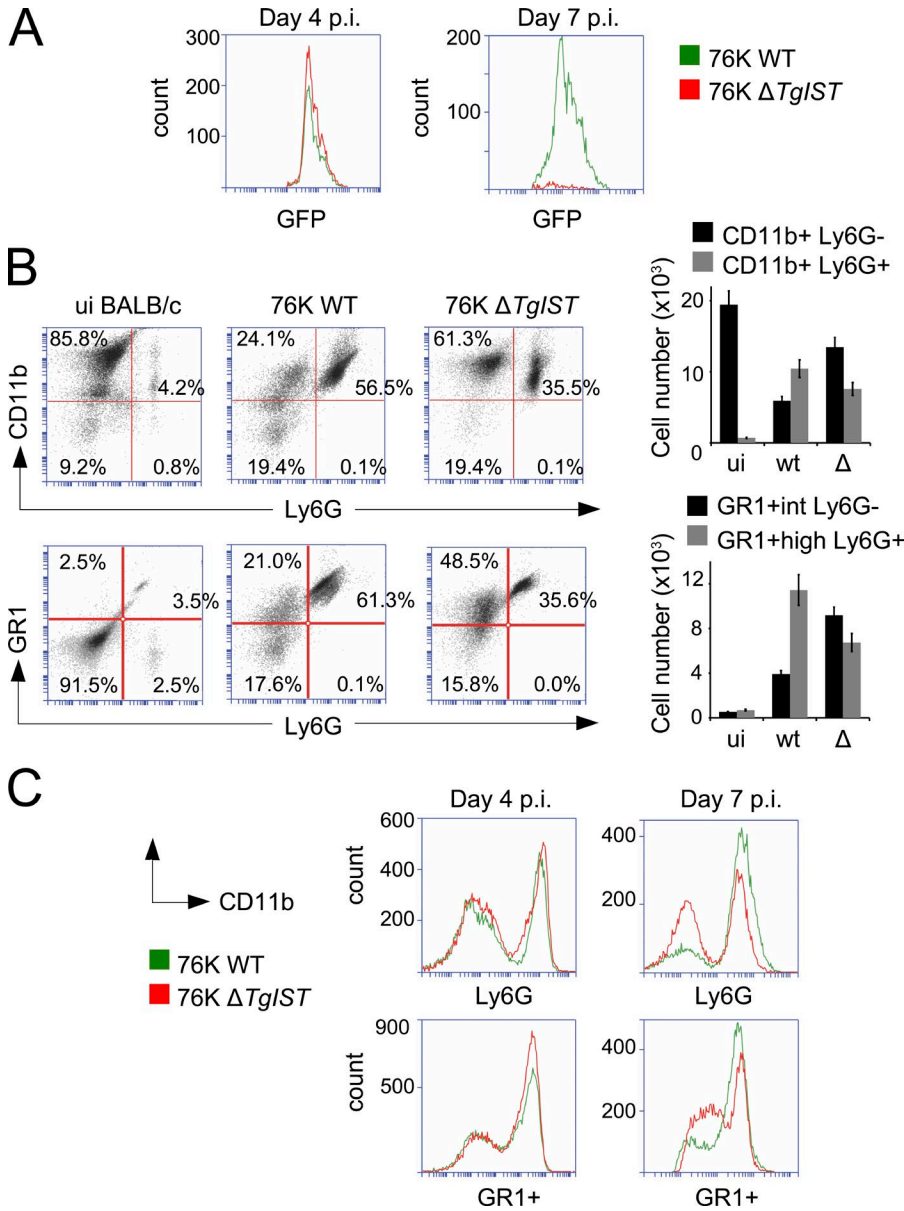


Figure 10. Flow cytometry analyses of myeloid cells in the peritoneal lavage fluids after inoculation to mice of either WT or *TgIST*-deficient parasites. (A) Flow cytometric detection of GFP-expressing parasites in the peritoneal lavage fluids collected from BALB/c mice at days 4 and 7 after inoculation of either 10^5 76K GFP WT or $\Delta TgIST$ tachyzoites. (B) Detection of Gr1⁺ proinflammatory macrophages and neutrophils in the peritoneal lavage fluids of mice after *T. gondii* infection. Cell populations were characterized and quantified by flow cytometry with anti-CD11b (conjugated to PE), anti-Ly6G (conjugated to APC), and anti-Gr1 (mAb RB6-8C5 conjugated to PE). Numbers indicate the percentage of cells within the gate. Histograms represent the absolute number of the aforementioned cells. Results are representative of two or more independent experiments ($n = 3$ animals were pooled for each) for all panels. Data shown are means \pm SD. (C) Flow cytometry quantification of CD11b⁺, Ly6G, and Gr1⁺ populations present at days 4 and 7 in the peritoneal lavage fluids collected from BALB/c mice to which were given i.p. either 10^5 76K GFP WT or $\Delta TgIST$ tachyzoites.

effectors downstream of IFN- γ , it became inefficient with time when most myeloid cells were already primed for their killing activity by the burst of cytokines prior infection (Fig. 8). Accordingly, we observed a rapid control of the *TgIST*-deficient parasites in mice (Fig. 9) that also concurred with a highly efficient i.p. homing of Gr1⁺ proinflammatory monocytes (Fig. 10). Thus, the time-restricted activity of TgIST *in vivo* seems compatible with the observation that mice deficient in STAT1 signaling remain highly susceptible to toxoplasmosis (Yap and Sher, 1999; Silva et al., 2002; Gavrilescu et al., 2004) and led us to assume that a TgIST-independent STAT1-dependent additional IFN- γ responsiveness is required to limit parasite propagation over time, thereby ensuring host survival.

It is noteworthy to mention that this work challenges the general view that nuclear STAT1 Y701-P obligatory signs

for active transcription. Indeed, we now show that the initiation of transcription of IFN- γ -stimulated genes can be impaired in the presence of STAT1 Y701-P bound to chromatin in the particular case of *T. gondii* infection. This arrest of transcription in infected cells only occurred if parasites secreted TgIST and if the latter formed such a tight complex with STAT1 that it prevented its dissociation from DNA (Fig. 7).

Importantly, because unchecked cytokine activation has dire consequences on tissue integrity, immune homeostasis requires negative feedback regulators. Regarding the JAK/STAT pathway, negative regulators fall into three groups, namely the SH2-containing phosphatases (SHPs), the suppressor of cytokine signaling (SOCS) proteins, and the protein inhibitor of activated STAT (PIAS) proteins, that all act by down-regulating the cytokine responses (Rakesh and

Agrawal, 2005). Our work reveals intriguing similarities in the modus operandi of TgIST and PIAS1, as the latter negatively regulates the expression of PIAS1-sensitive genes (including *Gbp1*) by enhancing promoter occupancy through a direct binding to STAT1 when cells are stimulated by IFN- γ (Liu et al., 2004). PIAS1-insensitive genes (including *Irf1*) were shown to be under the negative control of PIASy, which cooperates with PIAS1 to regulate the specificity and magnitude of STAT1-mediated gene activation (Tahk et al., 2007). Of note, *Pias1*-deficient mice displayed increased protection against both bacterial and viral infections (Liu et al., 2004) in line with the rapid recovery of mice infected with TgIST-deficient *T. gondii* (Fig. 9, A and B).

Gene transcription depends on the activation of HAT and inhibition of HDAC as both activities shape chromatin in a more open state. Interestingly, repression of the *T. gondii*-induced IFN- γ -stimulated gene was initially correlated with a reduced recruitment of HAT that resulted in hypoacetylated chromatin (Lang et al., 2012). In this respect, HDACs were shown to increase acetylation of histones and to favor the switch toward permissive chromatin of IFN- γ -activated cells (Lang et al., 2012). However, our data contradict this model. First, HDACi treatment did not alter *T. gondii*-mediated repression of IFN- γ -stimulated genes (unpublished data), in agreement with a previous study (Rosowski et al., 2014). Second, infection did not affect acetylated histone marks at *IRF1*, *CIITA*, and *CXCL10* loci regardless of TgIST presence or absence (Fig. 7 D), though the parasite effector firmly bound to both HDAC1 and HDAC2 (Fig. 2). We inferred that the aforementioned enzymes may play a positive role while associated to STAT1 and TgIST. For example, it was shown that HDAC activity is required to recruit RNA Pol II to the promoters of selected IFN- γ -stimulated early response genes (Sakamoto et al., 2004). An alternative explanation is that TgIST-bound HDAC prevents STAT1 acetylation and DNA dissociation, thereby reducing the pool of activation-competent STAT1 molecules in the cytosol and compromising a new round of STAT1-mediated transactivation (Krämer and Heinzel, 2010).

Even though HDAC enzymes do not contribute to alter the chromatin landscape, TgIST also bound to CHD 3 and 4 proteins that are both involved in NuRD-mediated transcriptional repression by influencing nucleosome positioning (Xue et al., 1998). Our current working model is that TgIST not only coopts transcriptionally competent STAT1 to target IFN- γ -dependent genes but also remodels the local environment by recruiting NuRD to create a nonpermissive chromatin state that shuts down RNA Pol II transcription. TgIST-mediated inhibition led to the paradoxical situation where H3K4me₃, a hallmark of activation, was sustainably enriched at STAT1-binding loci throughout infection. H3K4me₃ contributes with other histone modifications to mark bivalent chromatin domains known to promote the silencing of developmental genes while keeping them poised for rapid activation (Voigt et al., 2013; Matsu-

mura et al., 2015). TgIST-dependent H3K4me₃ enrichment at *IRF1* promoter was observed in both unstimulated and stimulated infected cells, suggesting that TgIST acts as a repressive “memory mark.”

We showed that TgIST-mediated gene silencing resulted in a prolonged nuclear retention of activated STAT1 at the level of GAS-containing promoter sites, concomitantly with H3K4me₃ enrichment. Because IFN- γ -mediated STAT1 activation is essential for the control of *T. gondii* growth, much effort has focused on understanding how the parasite can interfere with STAT1-mediated transcription in IFN- γ -treated cells. However, this study highlights that in the absence of IFN- γ stimulation, *T. gondii* infection triggered a significant increase of STAT1 Y701-P levels (Fig. 6 C, lanes 5 and 6). Because ROP16 directly tyrosine phosphorylates STAT3 and STAT6 (Saeij et al., 2007; Yamamoto et al., 2009), it is likely that the kinase also activates STAT1. ROP16 is highly polymorphic between type I (or III) and II parasites, and a single amino acid determines the strain difference in terms of STAT3 activation (Yamamoto et al., 2009). As shown previously (Rosowski and Saeij, 2012), we noticed that ROP16 from type I parasites contributed only to some extent to STAT1 Y701 phosphorylation, whereas controlled STAT3 phosphorylation was completely abrogated in cells infected with *Rop16*-deficient type I (RH) parasites and unstimulated cells (Fig. 6 D, lanes 2 and 4). Conversely, type II strain was unable to direct STAT3 phosphorylation but able to activate STAT1 in a ROP16-independent manner (Fig. 6 D, lanes 5 and 7). Intriguingly, lack of TgIST in either type I or II tachyzoites is sufficient to abrogate this phosphorylation (Fig. 6 C, lanes 9 and 10; and not depicted). Remarkably, ectopic expression of TgIST in mouse macrophages was sufficient to induce significant STAT1 Y701-P when compared with mCherry mock-transfected cells (Fig. 6 E). Moreover, TgIST-mediated activation was largely potentialized when IFN- γ was added (Fig. 6 E). Because TgIST shares no common structural domain with kinases (Fig. 1 A), it is therefore likely that the protein coopts a host kinase to shortcut the JAK-STAT signaling cascade and to promote a sustained STAT1-Y701 phosphorylation throughout infection.

With this study, we added to the growing list of *T. gondii* effectors TgIST, a protein that bridges host proteins to efficiently challenge the JAK/STAT canonical pathway, and in contrast to the IRG system that was lost in primates (Bekpen et al., 2005), this sophisticated type of molecular device appears ubiquitous in metazoans including humans and is likely to play a pivotal contribution to the pathophysiology of infectious diseases.

MATERIALS AND METHODS

Mice and experimental infection

6-wk-old BALB/cJrj mice were obtained from Charles River. Mouse care and experimental procedures were performed under pathogen-free conditions in accordance with established institutional guidance and approved protocols

from the institutional Animal Care and Use Committee of the University Grenoble Alpes (agreement #B3851610006).

Parasites and host cells

T. gondii strains were maintained in vitro by serial passage on monolayers of HFFs. The strains used in this study were RHku80, PruKu80, and 76K-GFP-LUC (gift of M. Grigg, National Institutes of Health, Bethesda, MD). HFF primary cells, RAW264.7, 2fTGH(STAT1^{+/+}), and U3A (STAT1^{-/-}; gift of J. Saeij, University of California, Davis, Davis, CA) cell lines were cultured in DMEM (Invitrogen) supplemented with 10% heat-inactivated FBS (Invitrogen), 10 mM Hepes buffer, pH 7.2, 2 mM L-glutamine, and 50 µg/ml penicillin and streptomycin (Thermo Fisher Scientific). A HEK-Blue IFN-γ responsive reporter cell line was cultured according to the manufacturer's instructions (InvivoGen).

Generation of mouse fibroblasts

Mouse primary fibroblasts were obtained from the tail (MTFs) and ears of female BALB/c mice. Biopsies were minced and incubated overnight in 400 U/ml collagenase type II (Sigma-Aldrich) dissolved in DMEM (Thermo Fisher Scientific) supplemented with 20% heat-inactivated FBS and incubated overnight at 37°C and 5% CO₂. Then, cells were dislodged from the digested tissues by repeated pipetting and were passed through 70-µm sterile netting into sterile 14-ml centrifuge tubes. The samples were centrifuged for 5 min at 350 g, and the cell pellet was resuspended in DMEM, 20% FBS, and further expanded in a 175-cm² cell culture flask. Cells were incubated at 37°C in 5% CO₂.

Generation of BMDMs

BMDMs were obtained from female C57BL/6 mice. BM was isolated by flushing hind tibias and femurs using a 25-gauge needle followed by passages through an 18-gauge needle to disperse cell clumps. Cells were suspended in DMEM supplemented with 10% heat-inactivated FBS and 20 ng/ml recombinant M-CSF (Invitrogen) and incubated in a tissue culture-treated flask for 8–12 h. Then, nonadherent cells were harvested and transferred in 55-cm² non-tissue culture-treated plates (Corning) at 4–6 × 10⁶ cells per plate and further incubated at 37°C, with 5% CO₂ in humidified air. After 6 d, cells were washed with PBS to remove nonadherent cells, harvested by dislodging with a cell scraper in ice-cold PBS, and replated for the assay. This method yielded a highly pure population of F4/80⁺ macrophages by immunofluorescence analysis (IFA).

Reagents

Antibodies against HA (3F10; Roche), IRF1 (D5E4; Cell Signaling Technology), STAT1 (Cell Signaling Technology), STAT1 Y701-P (Cell Signaling Technology), STAT1 S727-P (Cell Signaling Technology), STAT3 Y705-P (Cell Signaling Technology), USP7/HAUSP (A300-033A-3; Bethyl Laboratories, Inc.), CHD4 (3F2/4; Abcam), MTA1 (D40D1; Cell

Signaling Technology), HDAC1 (10E2; Cell Signaling Technology), RBBP7 (V415; Cell Signaling Technology), CTBP1 (Abcam), Toxofilin, TBP (Abcam), H3K4me3 (Diagenode), H3K9ac (17-658; EMD Millipore), anti-acetyl-Histone H4 (06-866; EMD Millipore), H3K27ac (17-683; EMD Millipore), and Irgb6 (gift of J. Howard, Instituto Gulbenkian de Ciência, Oeiras, Portugal) were used in immunofluorescence, immunoblotting, and/or ChIP assays. Immunofluorescence secondary antibodies were coupled with Alexa Fluor 488 or Alexa Fluor 594 (Thermo Fisher Scientific). Secondary antibodies used in Western blotting were conjugated to alkaline phosphatase (Promega). Recombinant human and mouse IFN-γ (Roche) were used to stimulate the aforementioned cells.

Immunofluorescence microscopy

Immunofluorescence assays were performed as described previously (Braun et al., 2013). In brief, cells grown on coverslips were washed in PBS and fixed for 20 min at room temperature with PBS containing 3% (vol/vol) formaldehyde. Fixed cells were permeabilized with PBS–0.1% Triton X-100 (vol/vol) for 10 min and blocked in PBS–3% BSA for 1 h at room temperature. Samples were incubated in PBS–3% BSA with the primary antibodies indicated in the figures, followed by the secondary antibodies coupled with Alexa Fluor 488 or Alexa Fluor 568 (Thermo Fisher Scientific) at a 1:1,000 dilution each in PBS–3% BSA. Nuclei of both host cells and parasites were stained for 10 min at room temperature with Hoechst 33258 at 2 µg/ml in PBS. After four washes in PBS, coverslips were mounted on a glass slide with Mowiol mounting medium. Images were acquired with a fluorescence microscope (Axio Imager 2_{apotome}; ZEISS).

Plasmid constructs

To construct the vector pLIC-TgIST-HA-DHFR, the coding sequence of TgIST was amplified using primers pLIC-HF-DHFR_F and pLIC-HF-DHFR_R using PruKu80 genomic DNA as template. The resulting PCR product was cloned into the pLIC-HF-dhfr vector using the LIC cloning method (Bougdour et al., 2013) yielding pLIC-TgIST-HA-DHFR. The plasmid pTOXO_Cas9-CRISPR::sgIST vector was generated as previously described (Curt-Varesano et al., 2016). In brief, primers TgIST-CRISP-FWD and TgIST-CRISP-REV containing the sgRNA targeting TgIST genomic sequence were phosphorylated, annealed, and ligated in the pTOXO_Cas9-CRISPR plasmid linearized with BsaI, yielding pTOXO_Cas9-CRISPR::sgTgIST. To construct the mammalian expression vector pcDNA4-HA-TgIST, TgIST coding sequence was amplified using primers pcDNA4-HA-TgIST_F and pcDNA4-HA-TgIST_R using PruKu80 genomic DNA as template. The resulting PCR product was cloned by LIC into the pcDNA-LIC-HF plasmid (Bougdour et al., 2013). Likewise, pcDNA4-TgIST-HA_F and pcDNA4-TgIST-HA_R primers were used to generate the plasmid pcDNA4-TgIST-HA, harboring a C-terminal HA tag.

***T. gondii* transfection**

Vectors were transfected into RHku80, PruKu80, and 76K-GFP-LUC tachyzoites by electroporation. Electroporation was performed in a 2-mm cuvette in a BTX ECM 630 (Harvard Apparatus) at 1,100 V, 25 Ω , and 25 μ F. Stable integrants were selected in media with 1 μ M pyrimethamine and cloned by limiting dilution.

Generation of the TgIST insertional mutant

Type I (RHku80) and II (PruKu80 and 76KGFP/LUC) were cotransfected with a mixture of the pTOXO_Cas9CRISP::sgIST vector with purified amplicons containing the DHFR cassette flanked by sequences homologous to the sequence targeted by sgIST. These amplicons were generated by PCR amplification of the DHFR cassette using the primers TgIST-DHFR-F and TgIST-DHFR-R and a vector carrying the DHFR cassette as template. To generate a complemented PruKu80 Δ TgIST strain, vector pLIC-P_{TgIST}-TgIST-HF was coelectroporated with the pMiniHX at 1:10 ratio, followed by selection with mycophenolic acid and xanthine, and cloned by limiting dilution. The resulting strain was named PruKu80 Δ TgIST, pLIC-P_{TgIST}-TgIST-HF (Table S1).

HEK-Blue IFN- γ cells transfection

24 h before transfection, the HEK-Blue IFN- γ cells (InvivoGen) were plated (80% confluency) in 24-well tissue culture dishes. 0.8 μ g HA fusion protein-expressing plasmids were transfected into cells with Lipofectamine 2000 (Thermo Fisher Scientific) according to the manufacturer's instructions. 24 h after transfection, IFN- γ was added at 100 U/ml, and the plates were incubated at 37°C for 24 h. 20 μ l of induced HEK-Blue IFN- γ cells supernatant was added to 180 μ l QUANTI-Blue. After incubating for 1–3 h at 37°C, the secreted embryonic alkaline phosphatase (SEAP) levels were determined using a spectrophotometer at 650 nm.

Chromatographic purification of TgIST-containing complexes

PruKu80_TgIST-HAFlag-infected host cell extracts containing Flag-tagged protein were incubated with anti-FLAG M2 affinity gel (Sigma-Aldrich) for 1 h at 4°C. Beads were washed with 10 column volumes of BC500 buffer (20 mM Tris-HCl, pH 8.0, 500 mM KCl, 10% glycerol, 1 mM EDTA, 1 mM DTT, 0.1% NP-40, 0.5 mM PMSE, and 1 μ g/ml each of aprotinin, leupeptin, and pepstatin). Bound peptides were eluted stepwise with 250 μ g/ml FLAG peptide (Sigma-Aldrich) diluted in BC100 buffer.

Mass spectrometry-based proteomics

Protein bands were excised from colloidal blue-stained gels (Thermo Fisher Scientific), treated with DTT and iodoacetamide to alkylate the cysteines before in-gel digestion using modified trypsin (sequencing grade; Promega). Resulting peptides from individual bands were analyzed by online

nanoLC-MS/MS (UltiMate 3000 coupled to LTQ-Orbitrap Velos Pro; Thermo Fisher Scientific) using a 25-min gradient. Peptides and proteins were identified and quantified using MaxQuant (version 1.5.3.17) through concomitant searches against ToxoDB (20151112 version), SwissProt (Homo sapiens taxonomy, 20151112 version), and the frequently observed contaminant database embedded in MaxQuant. Minimum peptide length was set to 7 amino acids. Minimum number of peptides, razor + unique peptides, and unique peptides were all set to 1. Maximum false discovery rates were set to 0.01 at peptide and protein levels.

Cell fractionation

For cytosolic and nuclear fractionation analysis, cells were washed in ice-cold PBS and harvested using a cell scraper. After centrifugation, cells were resuspended in buffer D (10 mM Hepes, pH 7.9, 10 mM KCl, 1.5 mM MgCl₂, 0.34 M sucrose, 10% glycerol, 1 mM DTT, and 1 \times Roche protease inhibitor cocktail) and lysed for 8 min with Triton X-100 at a final concentration of 0.1%. Cell lysates were centrifuged at 1,300 g for 5 min, and the supernatant containing the cytosolic fraction was collected. The pellet, containing the nuclear fraction, was washed once in buffer D and resuspended in cell extraction buffer (Thermo Fisher Scientific) for protein extraction. The supernatant and pellet fractions were clarified by centrifugation at 20,000 g for 10 min at 4°C. Supernatants were mixed with protein sample buffer (Thermo Fisher Scientific) for Western blot analysis.

Western blot

Proteins were separated by SDS-PAGE and transferred to a polyvinylidene fluoride membrane (Immobilon-P; EMD Millipore) by liquid transfer, and Western blots were probed using appropriate primary antibodies followed by phosphatase-conjugated goat secondary antibodies (Promega). Signals were detected using NBT-BCIP (Amresco).

Harvest of peritoneal contents, in vivo cytokine ELISA, and determination of parasite load

6-wk-old BALB/cJRj mice (Charles River) were i.p. infected with 10⁵ parasites and sacrificed on days 2, 5, 7, and 9 p.i. Immediately after being killed, mice were peritoneally lavaged with 3 ml of physiological serum. 2 ml of recovered lavage fluid was centrifuged at 20,000 g for 15 min at 4°C, and the clarified supernatant was stored at -80°C until analyzed by ELISA. IL-12, IFN- γ , and IL-1 β levels were determined using commercially available ELISA kits (IL-12 p40 ELISA kit [Thermo Fisher Scientific], IFN- γ ELISA kit [Thermo Fisher Scientific], and IL-1 β Quantikine ELISA kit [R&D Systems]). The parasite loads in peritoneal content were quantified after DNA extraction (QIAamp DNA mini kit; QIAGEN) using the quantitative PCR targeting of the *T. gondii*-specific 529-bp repeat element.

Quantitative real-time RT-PCR

Total RNA was isolated from infected cells using TRIzol (Thermo Fisher Scientific). cDNA was synthesized with random hexamers by using the High Capacity RNA-to-cDNA kit (Applied Biosystems). Samples were analyzed by real-time quantitative PCR for appropriate probes using TaqMan Gene Expression Master Mix (Applied Biosystems) according to the manufacturer's instructions. *β2-microglobulin* was used as an internal control gene.

ChIP assay

HFF cells were infected for 24 h with Pruku80TgIST-HAFlag and Pruku80 Δ TgIST and stimulated with 100 U/ml IFN- γ for 1 h or left unstimulated. Cells were then cross-linked with 1% formaldehyde for 10 min before quenching with 125 mM glycine for 5 min. The ChIP assay was performed by using the Transcription Factor Chromatin Immunoprecipitation kit (Diagenode) according to the manufacturer's protocol. In brief, fixed cells were sonicated to shear the cross-linked chromatin into a mean DNA fragment size of 200–600 bp. We used 40 million sorted nuclei in 300 μ l of immunoprecipitation buffer supplemented with fresh proteinase inhibitors. By using a Diagenode Bioruptor precooled to 4°C, shearing was achieved in 1.5-ml low binding tubes in the appropriate tube adapter with 18 high-energy cycles of 30 s on/30 s off. The aforementioned antibodies were used for immunoprecipitation. After overnight incubation, DNA–protein–antibody complex was eluted. The cross-links were reversed by heating the samples at 65°C for 4 h. DNA was purified by using IPure kit (Diagenode) according to the manufacturer's protocol. For validation, quantitative real-time ChIP-PCR was performed by SYBR Green (Applied Biosystems) using the StepOnePlus (Applied Biosystems). Real-time PCR was performed and then quantitated using the delta–delta CT ($\Delta\Delta$ CT) method. Primer sequences are listed in Table S1.

Bioluminescence imaging

Noninvasive bioluminescence imaging was performed 0, 2, 5, 7, and 10 d after *T. gondii* infection (5×10^4 tachyzoites). 5 min before imaging, vigil mice received an i.p. injection of 150 μ g/g of D-luciferin (Promega) and were then anesthetized (isoflurane 4% for induction and 1.5% thereafter) and placed in the optical imaging system (IVIS Kinetic; PerkinElmer). This allowed localization of luciferase-positive *T. gondii* and evaluation of the abdominal load. Bioluminescence signal was expressed as photons/seconds (p/s).

Flow cytometry

6-wk-old BALB/cJrj mice (Charles River) were i.p. infected with 10^5 parasites and sacrificed on days 4 and 7 p.i. Immediately after being killed, mice were peritoneally lavaged with PBS, and recovered lavage fluid was centrifuged at 500 g for 8 min. Peritoneal cells were washed in stain buffer (PBS containing 2% FBS and 0.1 mM EDTA), and cells were then pretreated at 4°C for 1 h with mAb 2.4G2

to block nonspecific binding to Fc γ receptors. Thereafter, cells were incubated for 1 h with fluorescently conjugated antibodies for cell surface markers from BD: PE-conjugated anti-CD11b, PE-conjugated anti-Gr1, PE-conjugated anti-CD11c, and APC-conjugated anti-Ly-6G. Isotype controls consisted of PE-conjugated rat IgG2b, PE-conjugated hamster IgG1, and APC-conjugated rat IgG2a, provided by BD. Analysis of stained cells was performed with a FACSCalibur flow cytometer (BD). For all samples, 100,000 cells were analyzed for plot generation.

Microarray hybridization and data analysis

HFFs, 2fTGH, and U3A were plated at $8\text{--}10 \times 10^6$ cells per 55-cm² plate, infected (MOI = 6) for 24 h with 76KG-FP-WT and Δ TgIST and with 100 U/ml IFN- γ for 6 h. RNA was isolated using TRIzol reagent, followed by phenol/chloroform/isoamyl extraction. RNA quantity and quality were measured by NanoDrop ND-1000. RNA integrity was assessed by standard denaturing agarose gel electrophoresis. Transcripts were obtained from three biological replicates each. Total RNA from each sample was linearly amplified and labeled with Cy3-UTP. The labeled cRNAs were purified by RNeasy Mini kit (QIAGEN). The concentration and specific activity of the labeled cRNAs (pmol Cy3/ μ g cRNA) were measured by NanoDrop ND-1000. 1 μ g of each labeled cRNA was fragmented by adding 11 μ l of $10\times$ blocking agent and 2.2 μ l of $25\times$ fragmentation buffer and then heated at 60°C for 30 min, and finally 55 μ l of $2\times$ hybridization buffer (GE Healthcare) was added to dilute the labeled cRNA. 100 μ l of hybridization solution was dispensed into the gasket slide and assembled to the gene expression microarray slide. The slides were incubated for 17 h at 65°C in a hybridization oven (Agilent Technologies). Feature extraction software (version 11.0.1.1; Agilent Technologies) was used to analyze the acquired array images. Quantile normalization and subsequent data processing were performed with using the GeneSpring GX version 12.1 software (Agilent Technologies). After quantile normalization of the raw data, genes that had at least 3 out of 27 samples have flags in Detected (“All Targets Value”) were chosen for further data analysis. Differentially expressed genes with statistical significance were identified through Volcano Plot filtering. Hierarchical clustering was performed using the R software (version 2.15). GO analysis and Pathway analysis were performed in the standard enrichment computation method. The thresholds were fold change ≥ 2.0 , p-value ≤ 0.05 . GO analysis and KEGG (Kyoto Encyclopedia of Genes and Genomes) pathway analysis were performed using the DAVID Bioinformatics Resources. GSEA and DIRE analysis were performed to identify TFBSs. Microarray data has been uploaded to GEO Datasets under accession no. GSE81613.

Online supplemental material

Table S1, included as an Excel file, describes all of the oligonucleotides, plasmids, and strains generated in this study.

Online supplemental material is available at <http://www.jem.org/cgi/content/full/jem.20160340/DC1>.

ACKNOWLEDGMENTS

We thank Dr. Geneviève Milon (Pasteur Institute) for her valuable comments. We thank Pr. Jonathan Howard (Lisbon) for his kind gift of the Irgb6 antibody.

This work was supported by the Laboratoire d'Excellence (LabEx) ParaFrap (ANR-11-LABX-0024), the European Research Council (ERC Consolidator Grant N° 614880 Hosting TOXO to M.-A. Hakimi), and Agence Nationale de la Recherche (ANR) grant ANR Blanc 2012 TOXOHADAC (ANR-12-BSV3-0009-01). Proteomic experiments were partly supported by the ANR (Investissement d'Avenir Infrastructures, ProFi project ANR-10-INBS-08-01).

The authors declare no competing financial interests.

Submitted: 3 March 2016

Accepted: 22 July 2016

REFERENCES

- Bekpen, C., J.P. Hunn, C. Rohde, I. Parvanova, L. Guethlein, D.M. Dunn, E. Glowalla, M. Leptin, and J.C. Howard. 2005. The interferon-inducible p47 (IRG) GTPases in vertebrates: loss of the cell autonomous resistance mechanism in the human lineage. *Genome Biol.* 6:R92. <http://dx.doi.org/10.1186/gb-2005-6-11-r92>
- Bougdour, A., E. Durandau, M.-P. Brenier-Pinchart, P. Ortet, M. Barakat, S. Kieffer, A. Curt-Varesano, R.-L. Curt-Bertini, O. Bastien, Y. Coute, et al. 2013. Host cell subversion by *Toxoplasma* GRA16, an exported dense granule protein that targets the host cell nucleus and alters gene expression. *Cell Host Microbe.* 13:489–500. <http://dx.doi.org/10.1016/j.chom.2013.03.002>
- Braun, L., M.-P. Brenier-Pinchart, M. Yogavel, A. Curt-Varesano, R.-L. Curt-Bertini, T. Hussain, S. Kieffer-Jaquinod, Y. Coute, H. Pelloux, I. Tardieux, et al. 2013. A *Toxoplasma* dense granule protein, GRA24, modulates the early immune response to infection by promoting a direct and sustained host p38 MAPK activation. *J. Exp. Med.* 210:2071–2086. <http://dx.doi.org/10.1084/jem.20130103>
- Chinnadurai, G. 2002. CtBP, an unconventional transcriptional corepressor in development and oncogenesis. *Mol. Cell.* 9:213–224. [http://dx.doi.org/10.1016/S1097-2765\(02\)00443-4](http://dx.doi.org/10.1016/S1097-2765(02)00443-4)
- Coffey, M.J., B.E. Sleebs, A.D. Uboldi, A. Garnham, M. Franco, N.D. Marino, M.W. Panas, D.J. Ferguson, M. Enciso, M.T. O'Neill, et al. 2015. An aspartyl protease defines a novel pathway for export of *Toxoplasma* proteins into the host cell. *eLife.* 4:e10809. <http://dx.doi.org/10.7554/eLife.10809>
- Collazo, C.M., G.S. Yap, S. Hieny, P. Caspar, C.G. Feng, G.A. Taylor, and A. Sher. 2002. The function of gamma interferon-inducible GTP-binding protein IGTP in host resistance to *Toxoplasma gondii* is Stat1 dependent and requires expression in both hematopoietic and nonhematopoietic cellular compartments. *Infect. Immun.* 70:6933–6939. <http://dx.doi.org/10.1128/IAI.70.12.6933-6939.2002>
- Curt-Varesano, A., L. Braun, C. Ranquet, M.-A. Hakimi, and A. Bougdour. 2016. The aspartyl protease TgASP5 mediates the export of the *Toxoplasma* GRA16 and GRA24 effectors into host cells. *Cell. Microbiol.* 18:151–167. <http://dx.doi.org/10.1111/cmi.12498>
- Dunay, I.R., R.A. Damatta, B. Fux, R. Presti, S. Greco, M. Colonna, and L.D. Sibley. 2008. Gr1⁺ inflammatory monocytes are required for mucosal resistance to the pathogen *Toxoplasma gondii*. *Immunity.* 29:306–317. <http://dx.doi.org/10.1016/j.immuni.2008.05.019>
- Etheridge, R.D., A. Alaganan, K. Tang, H.J. Lou, B.E. Turk, and L.D. Sibley. 2014. The *Toxoplasma* pseudokinase ROP5 forms complexes with ROP18 and ROP17 kinases that synergize to control acute virulence in mice. *Cell Host Microbe.* 15:537–550. <http://dx.doi.org/10.1016/j.chom.2014.04.002>
- Gavrilescu, L.C., B.A. Butcher, L. Del Rio, G.A. Taylor, and E.Y. Denkers. 2004. STAT1 is essential for antimicrobial effector function but dispensable for gamma interferon production during *Toxoplasma gondii* infection. *Infect. Immun.* 72:1257–1264. <http://dx.doi.org/10.1128/IAI.72.3.1257-1264.2004>
- Hakimi, M.-A., and A. Bougdour. 2015. *Toxoplasma's* ways of manipulating the host transcriptome via secreted effectors. *Curr. Opin. Microbiol.* 26:24–31. <http://dx.doi.org/10.1016/j.mib.2015.04.003>
- Honda, K., and T. Taniguchi. 2006. IRFs: master regulators of signalling by Toll-like receptors and cytosolic pattern-recognition receptors. *Nat. Rev. Immunol.* 6:644–658. <http://dx.doi.org/10.1038/nri1900>
- Howard, J.C., J.P. Hunn, and T. Steinfeldt. 2011. The IRG protein-based resistance mechanism in mice and its relation to virulence in *Toxoplasma gondii*. *Curr. Opin. Microbiol.* 14:414–421. <http://dx.doi.org/10.1016/j.mib.2011.07.002>
- Kim, S.-K., A.E. Fouts, and J.C. Boothroyd. 2007. *Toxoplasma gondii* dysregulates IFN- γ -inducible gene expression in human fibroblasts: insights from a genome-wide transcriptional profiling. *J. Immunol.* 178:5154–5165. <http://dx.doi.org/10.4049/jimmunol.178.8.5154>
- Krämer, O.H., and T. Heinzel. 2010. Phosphorylation-acetylation switch in the regulation of STAT1 signaling. *Mol. Cell. Endocrinol.* 315:40–48. <http://dx.doi.org/10.1016/j.mce.2009.10.007>
- Kravets, E., D. Degrandi, Q. Ma, T.-O. Peulen, V. Klümpers, S. Felekyan, R. Kühnemuth, S. Weidtkamp-Peters, C.A. Seidel, and K. Pfeffer. 2016. Guanylate binding proteins directly attack *Toxoplasma gondii* via supramolecular complexes. *eLife.* 5:e11479. <http://dx.doi.org/10.7554/eLife.11479>
- Lang, C., A. Hildebrandt, F. Brand, L. Opitz, H. Dihazi, and C.G.K. Lüder. 2012. Impaired chromatin remodelling at STAT1-regulated promoters leads to global unresponsiveness of *Toxoplasma gondii*-infected macrophages to IFN- γ . *PLoS Pathog.* 8:e1002483. <http://dx.doi.org/10.1371/journal.ppat.1002483>
- Liu, B., S. Mink, K.A. Wong, N. Stein, C. Getman, P.W. Dempsey, H. Wu, and K. Shuai. 2004. PIAS1 selectively inhibits interferon-inducible genes and is important in innate immunity. *Nat. Immunol.* 5:891–898. <http://dx.doi.org/10.1038/ni1104>
- Lüder, C.G., C. Lang, M. Giraldo-Velasquez, M. Algner, J. Gerdes, and U. Gross. 2003. *Toxoplasma gondii* inhibits MHC class II expression in neural antigen-presenting cells by down-regulating the class II transactivator CIITA. *J. Neuroimmunol.* 134:12–24. [http://dx.doi.org/10.1016/S0165-5728\(02\)00320-X](http://dx.doi.org/10.1016/S0165-5728(02)00320-X)
- Martens, S., I. Parvanova, J. Zerrahn, G. Griffiths, G. Schell, G. Reichmann, and J.C. Howard. 2005. Disruption of *Toxoplasma gondii* parasitophorous vacuoles by the mouse p47-resistance GTPases. *PLoS Pathog.* 1:e24. <http://dx.doi.org/10.1371/journal.ppat.0010024>
- Matsumura, Y., R. Nakaki, T. Inagaki, A. Yoshida, Y. Kano, H. Kimura, T. Tanaka, S. Tsutsumi, M. Nakao, T. Doi, et al. 2015. H3K4/H3K9me3 bivalent chromatin domains targeted by lineage-specific DNA methylation pauses adipocyte differentiation. *Mol. Cell.* 60:584–596. <http://dx.doi.org/10.1016/j.molcel.2015.10.025>
- McKendry, R., J. John, D. Flavell, M. Müller, I.M. Kerr, and G.R. Stark. 1991. High-frequency mutagenesis of human cells and characterization of a mutant unresponsive to both alpha and gamma interferons. *Proc. Natl. Acad. Sci. USA.* 88:11455–11459. <http://dx.doi.org/10.1073/pnas.88.24.11455>
- Meira, C.S., V.L. Pereira-Chioccola, J.E. Vidal, C.C.B. de Mattos, G. Motoie, T.A. Costa-Silva, R. Gava, F.B. Frederico, and L.C. de Mattos. *Toxoplasma* Groups. 2014. Cerebral and ocular toxoplasmosis related with IFN- γ , TNF- α , and IL-10 levels. *Front. Microbiol.* 5:492.
- Melo, M.B., K.D.C. Jensen, and J.P.J. Saeij. 2011. *Toxoplasma gondii* effectors are master regulators of the inflammatory response. *Trends Parasitol.* 27:487–495. <http://dx.doi.org/10.1016/j.pt.2011.08.001>

- Pereira-Chioccola, V.L., J.E. Vidal, and C. Su. 2009. *Toxoplasma gondii* infection and cerebral toxoplasmosis in HIV-infected patients. *Future Microbiol.* 4:1363–1379. <http://dx.doi.org/10.2217/fmb.09.89>
- Rakesh, K., and D.K. Agrawal. 2005. Controlling cytokine signaling by constitutive inhibitors. *Biochem. Pharmacol.* 70:649–657. <http://dx.doi.org/10.1016/j.bcp.2005.04.042>
- Ramana, C.V., M. Chatterjee-Kishore, H. Nguyen, and G.R. Stark. 2000. Complex roles of Stat1 in regulating gene expression. *Oncogene.* 19:2619–2627. <http://dx.doi.org/10.1038/sj.onc.1203525>
- Robben, P.M., M. LaRegina, W.A. Kuziel, and L.D. Sibley. 2005. Recruitment of Gr-1⁺ monocytes is essential for control of acute toxoplasmosis. *J. Exp. Med.* 201:1761–1769. <http://dx.doi.org/10.1084/jem.20050054>
- Robertson, A.G., M. Bilenky, A. Tam, Y. Zhao, T. Zeng, N. Thiessen, T. Cezard, A.P. Fejes, E.D. Wederell, R. Cullum, et al. 2008. Genome-wide relationship between histone H3 lysine 4 mono- and tri-methylation and transcription factor binding. *Genome Res.* 18:1906–1917. <http://dx.doi.org/10.1101/gr.078519.108>
- Rosowski, E.E., and J.P.J. Saeij. 2012. *Toxoplasma gondii* clonal strains all inhibit STAT1 transcriptional activity but polymorphic effectors differentially modulate IFN γ induced gene expression and STAT1 phosphorylation. *PLoS One.* 7:e51448. <http://dx.doi.org/10.1371/journal.pone.0051448>
- Rosowski, E.E., Q.P. Nguyen, A. Camejo, E. Spooner, and J.P.J. Saeij. 2014. *Toxoplasma gondii* inhibits gamma interferon (IFN- γ)- and IFN- β -induced host cell STAT1 transcriptional activity by increasing the association of STAT1 with DNA. *Infect. Immun.* 82:706–719. <http://dx.doi.org/10.1128/IAI.01291-13>
- Sadzak, I., M. Schiff, I. Gattermeier, R. Glinitzer, I. Sauer, A. Saalmüller, E. Yang, B. Schaljo, and P. Kovarik. 2008. Recruitment of Stat1 to chromatin is required for interferon-induced serine phosphorylation of Stat1 transactivation domain. *Proc. Natl. Acad. Sci. USA.* 105:8944–8949. <http://dx.doi.org/10.1073/pnas.0801794105>
- Saeij, J.P.J., S. Coller, J.P. Boyle, M.E. Jerome, M.W. White, and J.C. Boothroyd. 2007. *Toxoplasma* co-opts host gene expression by injection of a polymorphic kinase homologue. *Nature.* 445:324–327. <http://dx.doi.org/10.1038/nature05395>
- Sakamoto, S., R. Potla, and A.C. Lerner. 2004. Histone deacetylase activity is required to recruit RNA polymerase II to the promoters of selected interferon-stimulated early response genes. *J. Biol. Chem.* 279:40362–40367. <http://dx.doi.org/10.1074/jbc.M406400200>
- Scallan, E., R.M. Hoekstra, B.E. Mahon, T.F. Jones, and P.M. Griffin. 2015. An assessment of the human health impact of seven leading foodborne pathogens in the United States using disability adjusted life years. *Epidemiol. Infect.* 143:2795–2804. <http://dx.doi.org/10.1017/S0950268814003185>
- Scharton-Kersten, T.M., G. Yap, J. Magram, and A. Sher. 1997. Inducible nitric oxide is essential for host control of persistent but not acute infection with the intracellular pathogen *Toxoplasma gondii*. *J. Exp. Med.* 185:1261–1274. <http://dx.doi.org/10.1084/jem.185.7.1261>
- Schneider, A.G., D.S. Abi Abdallah, B.A. Butcher, and E.Y. Denkers. 2013. *Toxoplasma gondii* triggers phosphorylation and nuclear translocation of dendritic cell STAT1 while simultaneously blocking IFN γ -induced STAT1 transcriptional activity. *PLoS One.* 8:e60215. <http://dx.doi.org/10.1371/journal.pone.0060215>
- Silva, N.M., C.V. Rodrigues, M.M. Santoro, L.F. Reis, J.I. Alvarez-Leite, and R.T. Gazzinelli. 2002. Expression of indoleamine 2,3-dioxygenase, tryptophan degradation, and kynurenine formation during in vivo infection with *Toxoplasma gondii*: induction by endogenous gamma interferon and requirement of interferon regulatory factor 1. *Infect. Immun.* 70:859–868. <http://dx.doi.org/10.1128/IAI.70.2.859-868.2002>
- Stark, G.R., and J.E. Darnell Jr. 2012. The JAK-STAT pathway at twenty. *Immunity.* 36:503–514. <http://dx.doi.org/10.1016/j.immuni.2012.03.013>
- Sturge, C.R., and F.Yarovinsky. 2014. Complex immune cell interplay in the gamma interferon response during *Toxoplasma gondii* infection. *Infect. Immun.* 82:3090–3097. <http://dx.doi.org/10.1128/IAI.01722-14>
- Sullivan, W.J. Jr., and V. Jeffers. 2012. Mechanisms of *Toxoplasma gondii* persistence and latency. *FEMS Microbiol. Rev.* 36:717–733. <http://dx.doi.org/10.1111/j.1574-6976.2011.00305.x>
- Tahk, S., B. Liu, V. Chernishof, K.A. Wong, H. Wu, and K. Shuai. 2007. Control of specificity and magnitude of NF- κ B and STAT1-mediated gene activation through PIASy and PIAS1 cooperation. *Proc. Natl. Acad. Sci. USA.* 104:11643–11648. <http://dx.doi.org/10.1073/pnas.0701877104>
- Voigt, P., W.-W. Tee, and D. Reinberg. 2013. A double take on bivalent promoters. *Genes Dev.* 27:1318–1338. <http://dx.doi.org/10.1101/gad.219626.113>
- Wojciak, J.M., M.A. Martinez-Yamout, H.J. Dyson, and P.E. Wright. 2009. Structural basis for recruitment of CBP/p300 coactivators by STAT1 and STAT2 transactivation domains. *EMBO J.* 28:948–958. <http://dx.doi.org/10.1038/emboj.2009.30>
- Xue, Y., J. Wong, G.T. Moreno, M.K. Young, J. Côté, and W. Wang. 1998. NURD, a novel complex with both ATP-dependent chromatin-remodeling and histone deacetylase activities. *Mol. Cell.* 2:851–861. [http://dx.doi.org/10.1016/S1097-2765\(00\)80299-3](http://dx.doi.org/10.1016/S1097-2765(00)80299-3)
- Yamamoto, M., D.M. Standley, S. Takashima, H. Saiga, M. Okuyama, H. Kayama, E. Kubo, H. Ito, M. Takaura, T. Matsuda, et al. 2009. A single polymorphic amino acid on *Toxoplasma gondii* kinase ROP16 determines the direct and strain-specific activation of Stat3. *J. Exp. Med.* 206:2747–2760. <http://dx.doi.org/10.1084/jem.20091703>
- Yamamoto, M., M. Okuyama, J.S. Ma, T. Kimura, N. Kamiyama, H. Saiga, J. Ohshima, M. Sasai, H. Kayama, T. Okamoto, et al. 2012. A cluster of interferon- γ -inducible p65 GTPases plays a critical role in host defense against *Toxoplasma gondii*. *Immunity.* 37:302–313. <http://dx.doi.org/10.1016/j.immuni.2012.06.009>
- Yap, G.S., and A. Sher. 1999. Effector cells of both nonhemopoietic and hemopoietic origin are required for interferon (IFN)- γ - and tumor necrosis factor (TNF)- α -dependent host resistance to the intracellular pathogen, *Toxoplasma gondii*. *J. Exp. Med.* 189:1083–1092. <http://dx.doi.org/10.1084/jem.189.7.1083>
- Yarovinsky, F. 2014. Innate immunity to *Toxoplasma gondii* infection. *Nat. Rev. Immunol.* 14:109–121. <http://dx.doi.org/10.1038/nri3598>
- Zhao, Y., D.J.P. Ferguson, D.C. Wilson, J.C. Howard, L.D. Sibley, and G.S. Yap. 2009. Virulent *Toxoplasma gondii* evade immunity-related GTPase-mediated parasite vacuole disruption within primed macrophages. *J. Immunol.* 182:3775–3781. <http://dx.doi.org/10.4049/jimmunol.0804190>
- Zimmermann, S., P.J. Murray, K. Heeg, and A.H. Dalpke. 2006. Induction of suppressor of cytokine signaling-1 by *Toxoplasma gondii* contributes to immune evasion in macrophages by blocking IFN- γ signaling. *J. Immunol.* 176:1840–1847. <http://dx.doi.org/10.4049/jimmunol.176.3.1840>